

THE EFFECT OF *L*-PHENYLALANINE ON THE DORSOMEDIAL HYPOTHALAMUS
AND GALANIN RECEPTOR ACTIVATION

BY
DIWAN YASHPAL MINOCHA

A thesis submitted to the
Department of Biology
Mount Allison University
in partial fulfilment of the requirements for the
Bachelor of Science degree with Honours
April 21st, 2023

Abstract

The dorsomedial hypothalamus (DMH) is a collection of neurons in the hypothalamus responsible for a regulating satiety resulting from glutamate transmission across the synapse. Many G protein-coupled receptors (GPCRs) are expressed in the DMH and are responsible for glutamate transmission. Many of these receptors are also expressed in various tissues such as the duodenum, and when activated, are known to secrete a potent satiety hormone, cholecystokinin (CCK). One key stimulus for CCK release in the duodenum is *L*-Phenylalanine (*L*-Phe). The Rourke Lab has previously shown that *L*-Phe is able to activate various GPCRs, such as the galanin family receptors (GALR1-3) which are known to be present in the hypothalamus and have been implicated with mediating energy homeostasis. However, if *L*-Phe can activate these receptors in a concentration dependent manner is not well understood. Moreover, the effect of *L*-Phe in the DMH is not currently known. HTLA cells (HEK 293A derived cells expressing a tTA-dependent firefly luciferase reporter gene and a β -arrestin2-TEV fusion gene) were used to measure galanin receptor activation. Cells expressing GALR1 or GALR2 were treated with *L*-Phe or a control prior to assessment of activation. We hypothesized that *L*-Phe would dose-dependently activate the receptors through the β -arrestin recruitment pathway, confirming them as *bone fide* *L*-Phe receptors. Cells expressing GALR1 were activated by *L*-Phe in a dose-dependent manner, resulting in an EC₅₀ of 754.4 μ M. Whole cell patch clamp electrophysiology was performed on living neurons in the DMH to assess changes in neuronal activity in the presence of 1 mM *L*-Phe. When *L*-Phe was present, there was a decrease in glutamate transmission, a long-term decrease in synaptic strength, as well as a decrease in the frequency of action potential firing. Elucidation of the effects of *L*-Phe in the DMH helps further the understanding of the role of *L*-Phe in energy homeostasis, as the characterized decrease could result in a suppression of appetite. Characterization of *L*-Phe receptors could be useful drug targets for various metabolic disorders such as phenylketonuria.

Acknowledgements

First and foremost, I would like to thank my amazing supervisors Dr. Karen Crosby and Dr. Jillian Rourke for agreeing to co-supervise me this year and tackle a new project. Without their support, mentorship, and leadership, I would not have been able to accomplish what I did. Thank you both for always being available to help me with any problem that I was having. I can not express my gratitude to you both for everything that you have done for me. I would also like to extend a huge thank you to Dr. Andrea Morash for willing to be a part of my thesis committee on short notice.

To my lab members, thank you all very much for making this year in the lab memorable, and more importantly, enjoyable. To the GPCRgang (Gang Proudly Conducting Research) (SunMin Park, Grace Stapleton, Gawon Suh), I appreciate every moment that we spent in the back closet trying to figure out problems, and all of our early mornings or late nights spent in cell culture. To the Crosby Lab (Logan Grossman, Lara Swart), thank you both so much for all of the times that you have helped me when needed, and worked through problems with me. Without all of you, this project would not have been seen to fruition. Thank you to all of my friends throughout my five years here who have helped me with everything. You have all kept me sane and helped me in so many ways.

And finally, thank you to my family for supporting me through my five years and being so understanding when I would have to travel back and forth to Sackville at odd hours to complete experiments. Your unwavering support, encouragement, and advice throughout the completion of this degree is unmatched and I can not express enough how grateful I am.

My gratitude for all those who have helped me and supported me extends far beyond what I could even begin to say. Thank you.

-Diwan Minocha

List of Abbreviations

Abbreviation	Definition
7TM	7 Transmembrane
aCSF	Artificial Cerebro Spinal Fluid
AMP	Ampicillin
AMPA	Amino-3-hydroxy-5-methyl-4-isoxazolepropionic acid
ANOVA	Analysis of variance
β -arrestin	Beta Arrestin
β -gal	pCMV-beta-galactosidase
cAMP	Cyclic adenosine monophosphate
CCK	Cholecystokinin
CNS	Central Nervous System
DMEM	Dulbecco's Modified Eagle Medium
DMH	Dorsomedial Hypothalamus
DMSO	Dimethyl sulfoxide
eEPSC	Evoked Excitatory Post Synaptic Currents
FBS	Fetal Bovine Serum
GABA	γ -amino-butyric-acid
GDP	Guanosine diphosphate
GFP	Green Fluorescent Protein
GPCR	G-Protein Coupled Receptor
GTP	Guanosine triphosphate
HFS	High Frequency Stimulation
HTLA	Human embryonic kidney (HEK) cells expressing a tTA-dependent luciferase reporter and a β -arrestin2-TEV fusion gene
HTS	High Throughput Screening
MAPK	Mitogen Activated Protein Kinase
NMDA	N-methyl-d-aspartate
PBS	Phosphate buffered saline
PEI	Polyethyleneimine
<i>L</i> -Phe	L-Phenylalanine
PPR	Paired Pulse Ratio
PRESTO-Tango	Parallel Receptor-ome Expression and Screening via Transcriptional Output-TANGO
SEM	Standard Error of Mean
sEPSC	Spontaneous Excitatory Post Synaptic Currents
Veh	Vehicle

List of Figures

Figure 1.1. Schematic design of the Tango assay. Upon ligand binding in the extracellular space to the GPCR, β -arrestin and a TEV protease are recruited to cleave the tethered transcription factor (tTA). The transcription factor enters the nucleus and binds to the DNA to promote transcription of the luciferase enzyme. Image modified from Kroeze et al., (2015) and made using BioRender.

Figure 1.2. Neuronal receptor family activation. Fold change activation response of neuronal GPCRs to L-phenylalanine. Modified from Madeline Power.

Figure 2.1. Action potential characteristics measured in Clampfit. **A)** Representative trace of action potential analysis on step one and eight acquired from Clampfit. **B)** All action potential analyses were performed on the first action potential that was fired once the current clamp protocol was initiated. The threshold value was determined by taking the first derivative of the action potential that occurred first. All subsequent measurements (latency to fire, amplitude, half-width, and after-hyperpolarization amplitude) were measured from the threshold value using Clampfit software.

Figure 2.2. Example recording trace of excitatory post synaptic currents. Evoked excitatory post synaptic currents (eEPSC) were stimulated using a stimulating electrode twice every five seconds, at 0.2Hz 50ms apart.

Figure 2.3. Experimental outline of L-phenylalanine experiments. **A)** After 5 minutes of baseline recording with slices incubated in aCSF and picrotoxin, the 1 mM *L*-Phe solution was applied, and recording continued for 10 minutes. The 1 mM *L*-Phe solution was subsequently washed out using aCSF and picrotoxin for another 10 minutes. **B)** High frequency stimulation (HFS) was applied after 5 minutes of baseline recording with aCSF, picrotoxin, and 1 mM *L*-Phe continuously in the recording chamber, followed by cellular recording for an additional 25 minutes.

Figure 2.4. Experimental outline of the PRESTO-Tango Assay procedure. Day 1) Plating HTLA cells at 25,000 cells/well in a 96 well plate. Day 2) Cells are transiently transfected with the GPCR plasmid of choice and controls. Day 2) Six hours after transfection, the transfection mix is removed from the cells and replaced with serum free *L*-Phe free DMEM. Day 3) HTLA cells are treated with galanin or *L*-Phe. Day 4) HTLA cells are lysed with 1X firefly reporter lysis buffer and stored at -80°C . Day X) Receptor activity quantified via luciferase and β -gal assays using a BioTek Synergy HT luminescence reader and Gen5 software. Image made using BioRender.

Figure 2.5. Experimental outline of MTT Assay. Day 1) HTLA cells were plated as per the PRESTO-Tango assay above. Day 2) Cells were transiently transfected with the empty plasmid vector pBSK. Day 2) Six hours later, 100% cell media was replaced with *L*-Phe, serum free DMEM. Day X) 20, 44, and 68 hours post *L*-Phe starvation, MTT reagent was added. Day X) Four hours later, DMSO was added to the wells and agitated for five minutes before reading at A570 using a BioTek Synergy HT luminescence reader and Gen5 software. Image made using BioRender.

Figure 3.1 *L*-Phe free media does not alter cell viability. HTLA cells transfected with the empty vector plasmid pBSK for 18 hours prior to media exchange to Opti-MEM, DMEM without 10% FBS (SF), *L*-Phe free complete DMEM (PF with 10% FBS), and serum free *L*-Phe free DMEM (PF SF) and remained on for 24 hours (A), 48 hours (B), and 72 hours (C) prior to performing the MTT assay. Dotted lines indicate the average cell viability of Opti-MEM. Data are shown as percent viability compared to Opti-MEM and represented as mean \pm SEM ($n = 3$) and evaluated using an ordinary one-way ANOVA, with Holm-Šídák multiple comparisons testing where $\alpha = 0.05$.

Figure 3.2. *L*-Phe dose dependently activates galanin receptor type one. HTLA cells were treated with *L*-phe (0 mM to 60 mM) following transfection of galanin receptor type 1 (A) or type 2 (B). Dotted line indicates logEC₅₀ value of 2.878 (EC₅₀ = 754.4 μ M). The luciferase/ β -galactosidase activity (relative light units (RLU)) was determined and expressed relative to the vehicle as fold change and corrected using the blank luminescence. Data are represented as mean \pm SEM ($n=1$) and curves were fitted with linear regression using log(agonist) vs response. Ordinary one-way ANOVA corrected using Holm-Šídák multiple comparisons testing where $\alpha = 0.05$.

Figure 3.3. Galanin treatment did not activate receptor type one and two. HTLA cells (HEK 293 A derived cells expressing tTA-dependent firefly luciferase reporter gene and a β -arrestin2-TEV fusion gene) were treated with galanin (0 μ M to 3 μ M) following transfection of GALR1 (A) and GALR2 (B). The luciferase/ β -galactosidase activity (relative light units (RLU)) was determined and expressed relative to the vehicle as fold change and corrected for using the blank luminescence. Data are represented as mean \pm SEM ($n=1$) and the curves were fitted with linear regression using log(agonist) vs response.

Figure 3.4. HTLA cells expressing green fluorescent protein (GFP). (A) Green fluorescent protein (GFP) expression in HTLA cells. (B) Transmitted light image of HTLA cells transfected with GFP. Images obtained using EVOS microscope, scale bar of 400 μ m.

Figure 3.5. Galanin receptors are activated by galanin dissolved in TBS or DMSO. HTLA cells were transfected with galanin receptor family type 1 (A) or type 2 (B) and treated with galanin dissolved in TBS or DMSO at 0 μ M, 1 μ M and 10 μ M. Luciferase/ β -galactosidase activity (relative light units (RLU)) was determined and expressed relative to the vehicle as fold change. Data represented as mean \pm SEM ($n = 3$) and evaluated using a one-way ANOVA, corrected using Holm-Šídák multiple comparisons testing where $\alpha = 0.05$.

Figure 3.6. *L*-Phenylalanine decreases glutamate transmission in the dorsomedial hypothalamus. **A)** Representative cell depicting evoked excitatory post synaptic currents (eEPSC) in picoamps (pA) over time (min) at baseline (0-5 min), 1mM *L*-Phe application (5-15 min) and subsequent wash out (15-30 min). Data represented as mean +/- SEM and the dotted line indicates the average baseline amplitude. **B)** Summary data illustrating eEPSC amplitude normalized to baseline, with the addition of 1mM *L*-Phe, and washout with aCSF and picrotoxin. The dotted line represents the average baseline amplitude. **C)** Paired pulse ratio (PPR) comparison between baseline, 1mM *L*-Phe, and washout. Data evaluated using an ordinary one-way ANOVA comparing baseline (0-5 minutes) to 1mM *L*-Phe (10-15 minutes) and washout (20-25 minutes), corrected for using Holm-Šidák multiple comparisons testing where $\alpha = 0.05$.

Figure 3.7. *L*-Phe significantly decreases neuronal excitability in the DMH. **(A)** Representative action potential traces at an injected current of -30 mV (corresponding to step eight of ten of the current clamp steps protocol) and -100 mV (corresponding to step one of ten). **(B)** Frequency of action potentials fired at an injected current of -30 mV. Data represented as mean +/- SEM for each of baseline, 1 mM *L*-Phe application, and subsequent washout.

Figure 3.8. *L*-Phe decreases latency to fire but does not alter alternative properties of action potentials. **(A)** A significant decrease in the latency to fire was observed in 1mM *L*-Phe and washout when compared to the baseline conditions. The **(B)** threshold was determined from the first derivative of the first action potential fired when current clamp steps protocol was initiated. The **(C)** peak amplitude **(D)** half-width, and **(E)** after hyperpolarization amplitude were all obtained from the threshold value, and there was no significant difference noted in these values.

Figure 3.9. Glutamate synapses undergo long-term depression following HFS in the presence of *L*-Phe. **(A)** Evoked excitatory post synaptic currents (eEPSC) of a representative control cell that has undergone high frequency stimulation (HFS) indicated by an arrow. **(B)** Summary of all recorded control cells showing the percent change in amplitude of eEPSC over time. **(C)** Paired pulse ratio (PPR) comparisons between baseline and post-HFS of control data. All control data was collected by Tenea Welsh. **(D)** Representative cell that has undergone high frequency stimulation (HFS) indicated by an arrow, in the presence of *L*-Phe. Illustrated above the graph are representative evoked excitatory traces. Dotted line indicates average baseline current amplitude in picoamps (pA). **(E)** Graphs depicting the eEPSC as a percent change from baseline of cells that underwent HFS, indicated by an arrow in the presence of *L*-Phe. **(F)** Paired pulse ratio (PPR) comparisons between baseline and post HFS in the presence of *L*-Phe. Dotted line indicates average baseline current amplitude in picoamps (pA).

Table of Contents

Abstract	II
Acknowledgements	III
List of Abbreviations	IV
List of Figures	V
Chapter 1: Introduction	1
1.1 <i>G Protein-Coupled Receptors</i>	1
1.2 <i>Cellular signalling</i>	2
1.3 <i>Using β-arrestin to study GPCR activation- the PRESTO-Tango Approach</i>	3
1.4 <i>L-Phenylalanine</i>	4
1.5 <i>Galanin Receptor Family 1 & 2</i>	6
1.6 <i>The Dorsomedial Hypothalamus</i>	6
1.7 <i>Neuronal Signalling</i>	7
1.8 <i>The Current Study</i>	8
Chapter 2: Methods	9
2.1 <i>Experimental Animals</i>	9
2.2 <i>Brain Removal and Slice Preparation</i>	9
2.3 <i>Patch-Clamp Electrophysiology</i>	9
2.4 <i>Experimental Outline for Electrophysiology Experiments</i>	12
2.5 <i>Cell Culture</i>	14
2.6 <i>Plasmid preparation</i>	14
2.7 <i>PRESTO-Tango assay</i>	14
2.7.1 <i>Plating</i>	16
2.7.2 <i>Transfection and L-Phenylalanine Starvation</i>	16
2.7.3 <i>Treatment</i>	16
2.7.4 <i>Cell Lysis</i>	17
2.7.5 <i>Beta gal and Luciferase assay</i>	17
2.8 <i>MTT Assay</i>	17
2.9 <i>Statistical Analysis</i>	18

Chapter 3: Results	20
3.1 <i>L-Phenylalanine free media does not alter cell viability.....</i>	20
3.2 <i>L-Phenylalanine dose dependently activates galanin receptor type one.....</i>	22
3.3 <i>Galanin in TBS or DMSO activates GALR1 and GALR2.....</i>	25
3.4 <i>L-Phenylalanine reduces glutamate transmission in the DMH of male rats.....</i>	26
3.5 <i>L-Phenylalanine does not significantly alter neuronal excitability at neurons in the DMH</i>	28
3.6 <i>A long term decrease in synaptic strength occurs as a result of L-Phe.....</i>	31
Chapter 4: Discussion	34
References.....	39
Appendix.....	47

Chapter 1: Introduction

1.1 G Protein-Coupled Receptors

G-Protein coupled receptors (GPCRs) are the most abundant cell membrane receptors. They are seven transmembrane (7TM) proteins with three intracellular and three extracellular loops ¹. Approximately 60 to 70% of drug targets are GPCRs, largely due to their high abundance, ligand diversity, and their ability to regulate various physiological functions including satiety^{2,3}. There are various endogenous and exogenous ligands for GPCRs including proteins, photons, odorants, ions, and neurotransmitters which can act as inhibiting antagonists or activating agonists ⁴. Orphan GPCRs are receptors that lack a known endogenous ligand, or do not have a known function, and therefore are an important target in pharmacological discoveries ⁵.

GPCRs are categorized into six families, A through F, based on their ligand, sequence, and physiological function ⁶. Classes A) rhodopsin, olfactory, and, adrenergic receptors, B) secretin receptors, C) metabotropic glutamate receptor family and F) frizzled or smoothed are all known to be present in humans ^{2,7}. Classes D and E are the fungal mating pheromone, and cyclic adenosine monophosphate (cAMP), respectively, and are not found in humans ⁸. Class A GPCRs are the largest family containing over 600 different receptors, and contain their ligand binding pocket within the 7TM region ^{6,9}. The intracellular loops and 7TM region are highly conserved in this class of GPCRs; however, members of this class detect a diversity in ligands. The diversity in ligand binding of class A GPCRs has been important in understanding the signalling pathways occurring in GPCRs ¹⁰. The β_2 adrenergic receptor (β_2 -AR) was the first neurotransmitter GPCR to be characterized by radioligand binding, have its structure determined by crystallography, and the first to be cloned ^{10,11}. Furthermore, ligand binding assays for β_2 -AR have been performed and have shown, when activated, this receptor is able to recruit the stimulatory G-protein (*Gas*) and act as the foundation for ternary complex formation upon ligand binding ¹². These initial findings on β_2 -AR contributed to its use as a model GPCR to help elucidate signalling events occurring in other GPCRs.

1.2 Cellular signalling

There are four distinct interlinked events that are the basis of cellular communication that allow cells to adapt to a given environment. 1) Primary messengers, known as ligands, travel from one cell to another and enter the extracellular space or bind to the receptor on the cell membrane. The ligand could be a protein on an adjacent cell, a hormone, antigen, neurotransmitter, amino acid, and much more¹³. 2) The receptor can be intracellular or on the cell membrane. After binding of the ligand to the receptor, the receptor undergoes a conformational change. 3) This conformational change initiates a signalling cascade which is responsible for various functions within the cell¹⁴. Finally, 4) the function of the target protein is altered when the signalling pathway is initiated^{13,14}.

Recruitment of G-proteins to the GPCR upon ligand binding was characterized by β_2 -AR due to its recruitment of the $G_{\alpha s}$ stimulatory G-protein and activation of the cAMP pathway¹⁰. This acted as the foundation for a canonical pathway such that upon ligand binding, G-proteins are recruited to the GPCR, forming a complex and subsequently activating downstream signalling pathways¹⁵.

A variety of G-proteins are primarily responsible for the transduced signal dictated by the binding of a ligand¹⁵. The different G-protein subunits associated with GPCRs are denoted alpha (α), gamma (γ), and beta (β). The α , β and γ subunits form a complex bound to the plasma membrane in the intracellular space by lipid anchors. When the GPCR is in its inactive state, a guanosine diphosphate (GDP) molecule is bound to the α subunit of the heterotrimeric G-protein. Upon ligand binding, the receptor acts as a guanine nucleotide exchange factor (GEF), replacing the GDP with GTP which activates the ensuing signal transduction cascade.

The GPCR is now able to initiate downstream signaling events through binding of various G-proteins, β -arrestin, and other pathways. The GTP- α complex is now in the intracellular space and recruits additional G-proteins to contribute to gene expression, cytokine production, tissue repair, and much more. G_i and G_s protein recruitment are responsible for inhibiting and activating adenylylate cyclase respectively. Cyclic adenosine monophosphate (cAMP), a secondary messenger in cellular signaling, is then activated and acts on protein kinase A (PKA) to help phosphorylate proteins important for gene expression

and regulation. After the G-proteins have bound, β -arrestin will bind to GPCR and promote internalization of the GPCR via the clathrin pit¹⁶. However, the description of β -arrestin has evolved over time to include its ability to activate the mitogen activated protein kinase (MAPK) pathway to contribute to other downstream mechanisms^{17,18}. β -arrestin signaling is important in ligand elucidation of orphan GPCRs because a large quantity of the known GPCRs are able to induce β -arrestin signalling^{17,19,20}.

1.3 Using β -arrestin to study GPCR activation- the PRESTO-Tango Approach

GPCRs have a variety of signal transduction cascades that are largely dependent on G-proteins, and vary by both the receptor and the ligand, thereby increasing the difficulty of high throughput screening (HTS) and identification of ligands for orphan receptors. Barnea *et al.*, sought to resolve this by developing the Tango assay, a β -arrestin proximity assay. This new HTS approach was improved by Kroeze *et al.*, (2015) who developed the Parallel Receptor-ome Expression and Screening *via* Transcriptional Output-TANGO (PRESTO-Tango) approach. The development of this assay allowed for HTS of known GPCRs to aid in their de-orphanization.

The Tango assay utilizes G-protein independent signalling such that when a ligand binds to the GPCR, a β -arrestin bound to Tobacco etch virus (TEV) protease is recruited. The β -arrestin-TEV cleaves the tethered transcription factor (tTA) allowing it to enter the nucleus and transcribe the luciferase enzyme (Figure 1.1)²². *D*-luciferin is the substrate for the luciferase enzyme, and when binding occurs, produces light. Luminescence can be quantified as a relative light level, and further indicate receptor activation²³. This is a highly powerful approach that is used to look at endogenous ligands, and orphan receptors in an attempt to de-orphanize them through a G-protein independent pathway. Specifically, the use of metabolites as agonists for GPCRs has been an emerging area of research especially amino acids, among which *L*-Phenylalanine is a top contender^{24,25}.

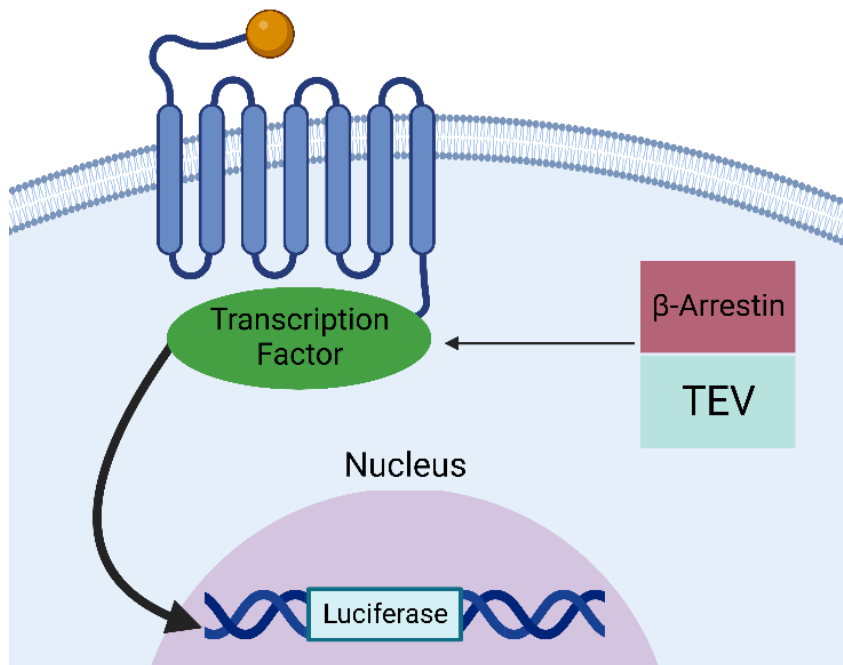


Figure 1.1. Schematic design of the Tango assay. Upon ligand binding in the extracellular space to the GPCR, β -arrestin and a TEV protease are recruited to cleave the tethered transcription factor (tTA). The transcription factor enters the nucleus and binds to the DNA to promote transcription of the luciferase enzyme. Image modified from Kroeze et al., (2015) and made using BioRender.

1.4 L-Phenylalanine

Amino acids serve a wide range of functions from acting as molecular precursors to hormones and neurotransmitters, to serving as building blocks in protein synthesis²⁶. L-Phenylalanine (*L*-Phe) is an essential amino acid with a number of functions: being used as a therapeutic to treat depression and ADHD^{27,28}, converted to *L*-tyrosine via phenylalanine hydroxylase and further to dopamine by DOPA carboxylase²⁹, as well as being a fundamental building block for protein synthesis²⁶. When there is a deficiency in the enzyme phenylalanine hydroxylase (PAH) which is responsible for metabolizing *L*-Phe to tyrosine³⁰ a build up of *L*-Phe occurs in the brain and is referred to as phenylketonuria (PKU). This neurological disorder results in neurodegenerative and neurodevelopmental problems if not treated³¹.

Beyond the well-known roles of *L*-Phe such as protein synthesis and catabolism, *L*-Phe has a number of putative roles. *L*-Phe is known to stimulate the release of satiety hormones from the gastrointestinal tract following a meal. For example, *L*-Phe triggers the release of cholecystokinin (CCK) from the small intestine in rats through a calcium-dependent pathway involving calcium-sensing receptors³²⁻³⁴. CCK is also able to act in the brain to suppress appetite³⁵; however, the effect of *L*-Phe in the brain, and its potential satiation effects remains unknown.

It has been previously established by the Rourke Lab that there are a variety of neuronal GPCRs that are activated by *L*-Phe through the β -arrestin recruitment pathway and all have important roles in the brain and satiety such as the corticotropin releasing hormone receptors and galanin receptors³⁶ (Figure 1.2).

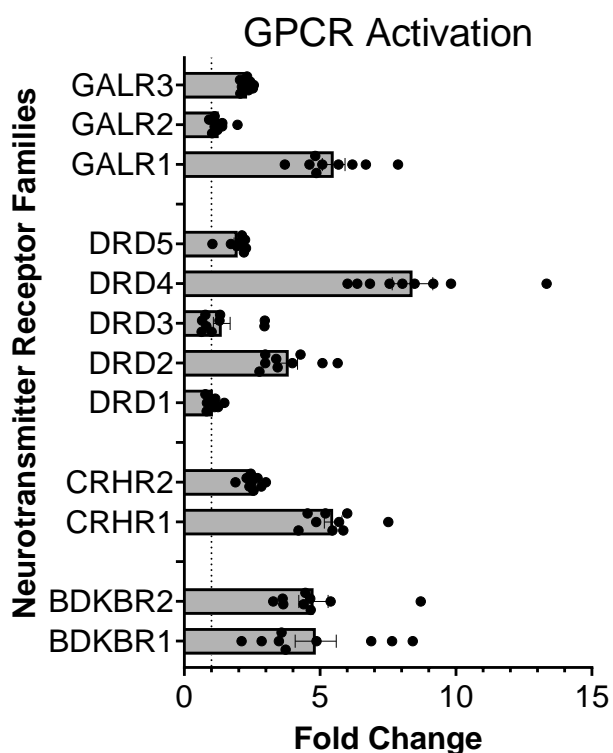


Figure 1.2. Neuronal receptor family activation. Fold change activation response of neuronal GPCRs to *L*-phenylalanine. Modified from Madeline Power.

1.5 Galanin Receptor Family 1 & 2

The galanin receptors are a family of three structurally similar GPCRs, GALR1-3, that detect the peptide ligand galanin. The galanin receptors are expressed widely in the central and peripheral nervous systems, specifically in the hypothalamus. The N-terminus of galanin is highly conserved amongst all species as it is primarily responsible for binding to the receptor. Murine galanin is 29 amino acids long while human galanin is 30 amino acids long³⁷. GALR1, and GALR2 are of particular interest in *L*-Phe signaling because of the physiological effect that these receptors have. In rats, galanin activation of GALR1 and GALR2 increases fat consumption and increases the expression of GALR, further increasing the feeding rate in rats^{38,39}. Importantly, GALR1 and GALR2 are well known for being present in the dorsomedial hypothalamus (DMH) and influencing satiation^{39,40}.

1.6 The Dorsomedial Hypothalamus

Located dorsal to the pituitary gland and adjacent to the third ventricle, the dorsomedial hypothalamus (DMH) is essential in homeostatic processes including appetite regulation, metabolism, thermoregulation, circadian rhythms, and the stress response^{35,41-44}. This homeostatic regulation is accomplished by neuronal communication between the DMH and other brain regions, both within the hypothalamus and beyond. The superchiasmatic nucleus, for example, has efferent projections to the DMH and contribute to the alterations in circadian rhythms and feeding behaviour of rats⁴².

Notably, the DMH contains efferent neurons to the paraventricular nucleus (PVN) and is largely responsible for maintaining energy homeostasis in rats^{42,44-47}. There is extensive evidence that the DMH is important in appetite regulation. Early lesioning studies in the DMH demonstrated that rats eat significantly less in the absence of DMH signaling⁴⁸. More recent optogenetic studies have supported the idea that DMH neurons stimulate appetite⁴⁴. Numerous studies also show that hormones can act in the DMH to influence food intake. Administration of CCK onto the DMH of young male rats has been found to decrease feeding and body weight through a CCK2 receptor and nitric oxide-mediated pathway⁴⁹. Changes in synaptic plasticity are known to occur within the DMH and PVN in response to food. One example involves an increase in synaptic strength between the DMH and PVN when rats were subjected to an overnight fast, and subsequently refed⁴⁵. This suggests that the connection between the DMH and the PVN is involved in alterations in food consumption and may further

help to mediate the metabolic affects of the ingested food ⁴⁵. Galanin is known to be heavily present in the central nervous system (CNS) and plays a role in food consumption. Direct administration of galanin into the lateral ventricle or the PVN induces feeding behaviour in rats ³⁸. Activation of galanin receptors is likely to contribute to this effect as both GALR1 and GALR2 are expressed in the DMH, and have been implicated in satiation ^{40,50,51}.

Taken together, these studies suggest that both the DMH and galanin receptor activation are implicated with satiety. It is possible that *L*-Phe can bind to galanin receptors to induce satiety through neuronal changes. However, the effect that *L*-Phe has on glutamate transmission in the DMH and the potential contributors to this effect are poorly understood.

1.7 Neuronal Signalling

Neurons, the foundational unit of the nervous system, use chemical and electrical signals to carry out a wide range of important physiological functions . Chemical neurotransmitters are typically released from the axon terminal of one neuron (pre-synaptic neuron) into the synaptic cleft, where they subsequently act on the dendrites of another (post-synaptic neuron) ⁵². Neurotransmitters bind to receptors and either open ion channels or trigger intracellular signaling cascades . Two of the major neurotransmitters in mammals are γ -aminobutyric acid (GABA) and glutamate, which are inhibitory or excitatory transmitters respectively ⁵³. Glutamate can bind to ionotropic receptors, including N-methyl-d-aspartate (NMDA), amino-3-hydroxy-5-methyl-4-isoxazolepropionic acid (AMPA), and kainate receptors, to trigger rapid excitatory effects ⁵⁴. Additionally, metabotropic GPCRs are known to bind glutamate and stimulate a corresponding stimulatory or inhibitory affect depending on the receptor ⁵⁵. Upon binding of ligand gated ion channels, a rapid influx of Na^+ and efflux of K^+ occurs, depolarizing the cell and making it more likely to fire an action potential. The action potential then travels along the axon and depolarizes the axon terminal, opening voltage gated Ca^{2+} channels and promoting the release of neurotransmitters. The released neurotransmitters travel through the synapse, a fundamental aspect of neuronal signalling. The synapse can undergo short or long-lasting changes in strength in response to various stimuli, referred to as synaptic plasticity ⁵⁶. Two types of synaptic plasticity are long-term depression (LTD) which is known to weaken the connections between neurons, and long-term potentiation (LTP) which strengthens the connections between synapses ⁵⁷. Both LTD and

LTP can be assessed by applying high frequency stimulation (HFS) to neurons and comparing the change in current amplitude before and after HFS application ³⁵.

1.8 The Current Study

Previous studies identified the dorsomedial hypothalamus as an important regulator in appetite ^{32,35,43,58,59}. Although the exact neural mechanisms are not fully understood, there is evidence that various hormones, including galanin and CCK act in the DMH to control appetite ^{32,51,60}. Interestingly, *L*-Phe can trigger the release of CCK and has been shown to activate galanin receptors.

L-Phe depresses glutamate transmission in the hippocampus and cerebral cortex of new born rats ⁶¹, however, little is currently known about the effect of *L*-Phe in the DMH. We aimed to characterize the effect of *L*-Phe on neuronal activity of glutamatergic synapses by assessing current amplitude, and action potential firing of living neurons using whole cell patch clamp electrophysiology.

Further, the Rourke lab has previously shown that *L*-Phe can activate various GPCRs including GALR 1, 2, and 3 which are expressed in the central nervous system and have been shown to influence food intake. However, little is currently known regarding the interaction between *L*-Phe and various GPCRs. We hope to build on this growing knowledge by performing PRESTO-Tango assays assessing the interaction of *L*-Phe with GPCRs seen through the β -arrestin recruitment pathway for each receptor, therefore confirming these receptors as *bone fide* *L*-Phe receptors.

Gaining an understanding of the effect of *L*-Phe on neuronal activity contributes to the growing knowledge of the role of nutrient signaling, specifically amino acids, in energy homeostasis. Additionally, identified receptors could pose as potential drug targets that are frequently noted in neurodevelopmental and degenerative disorders typically seen with PKU ³¹.

Chapter 2: Methods

2.1 Experimental Animals

Young, male Sprague-Dawley rats were obtained from Charles River Laboratories (Montreal Quebec, Canada) and arrived at Mount Allison University between 21 and 23 days old. Experimental procedures were conducted between 28 and 40 days old after the animals had time to acclimate to the environment. Animals were provided food (standard chow) and water *ad libitum*. The animals were housed in polycarbonate cages in groups of three to four that were filled with wood shavings, wood blocks, a Nylabone, and plastic hideout balls for environmental enrichment. The cages were housed in rooms held at 21°C and 50% humidity (+/- 10%) and were on a 12-hour light/dark cycle starting at 07:30. All experimental procedures were approved by the Mount Allison University Animal Care Committee under protocol number 103088, in accordance with the Canadian Council for Animal Care guidelines.

2.2 Brain Removal and Slice Preparation

To prepare for whole-cell electrophysiological recordings, brains were removed between 09:00 and 11:00. Animals were anesthetized using 5% isoflurane gas in oxygen in a secure chamber, supplemented with 3 mL of liquid isoflurane poured into the chamber. Once breathing subsided and reflexes ceased, animals were quickly placed in a guillotine to remove the head. The brain was quickly excised and placed in slushy slicing solution on ice, containing (in mM) 87 NaCl, 2.5 KCl, 25 NaCHO₃, 0.5 CaCl₂ • 2H₂O, 7 MgCl₂ • 6H₂O, 1.25 NaH₂PO₄, 25 glucose, and 75 sucrose, bubbled with 95% O₂/5% CO₂. A Leica vibratome (VT1000S) was used to create 250µm coronal slices which were incubated for a minimum of 60 minutes in artificial cerebrospinal fluid (aCSF) containing (in mM) 126 NaCl, 2.5 KCl, 26 NaCHO₃, 2.5 CaCl₂ • 2H₂O, 1.5 MgCl₂ • 6H₂O, 1.25 NaH₂PO₄, and 10 glucose, and bubbled with 95% O₂/5% CO₂.

2.3 Patch-Clamp Electrophysiology

Once the brain slices had recovered in aCSF, one slice was placed in the recording chamber of an Olympus upright water immersion microscope (BX51WL) equipped with infrared differential interference contrast optics (IR-DC) and attached to an Infinity2 camera to visualize the slices and locate the DMH adjacent to the third ventricle. Oxygenated aCSF at 32°C was superfused through the recording chamber at a rate of approximately 1 mL/min

to keep the cells healthy while recording. Borosilicate glass microelectrodes were pulled using a P-2000 pipette puller (Sutter instruments) with a tip resistance of 4.0-6.0 M Ω . A stimulating electrode was filled with aCSF and positioned near the cell of interest using a micromanipulator. A recording electrode was filled with an internal solution containing (in mM) 108 KGlucuronate, 8 KCl, 8 NaGlucuronate, 10 HEPES, 1 K₂ETGA, 2 MgCl₂, 4 K₂ATP, 0.3 Na₃GTP, corrected to a pH of 7.2 using KOH and an osmolarity of 280-300 mOsm using sterile water.

To achieve access to the cell, positive pressure was added to the recording electrode. Using a micromanipulator, the recording electrode was positioned such that the tip of the electrode was pressing against the cell of interest to form an indent on the membrane. The positive pressure was then released, suctioning the cell to the electrode and the membrane was broken by applying small bursts of negative pressure to gain access to the cell for whole-cell recordings. Access resistance was monitored every five minutes throughout the recording to monitor cell health. If access resistance had deviated by more than 20% from the initial access resistance, the cell would not be included in data analysis.

Once a cell was successfully patched, electrophysiological signals were digitized using a Digidata 1322 (Molecular Devices), amplified using a Multiclamp 700B amplifier (Molecular Devices) and filtered at 1kHz. Excitatory (glutamate) currents were recorded in the presence of picrotoxin (100 μ M in aCSF) to inhibit GABA_A receptors.

For each cell, action potentials were recorded in response to a series of depolarizing steps by injecting current into the cell using current clamp mode in the Clampex software, using the Multiclamp Commander. Cells were depolarized from -100 mV to -10 mV for 500 ms each, across a series of ten steps.

The number of action potentials was measured, along with the amplitude, threshold, latency to fire, half-width, and after-hyperpolarization amplitude (Figure 2.1). The first derivative was taken of the first action potential fired once the current clamp protocol was initiated and the threshold value was determined. All subsequent measurements (latency to fire, amplitude, half-width, and after-hyperpolarization amplitude) were measured from the threshold value using Clampfit software. The number of action potentials was reported as frequency and in one step.

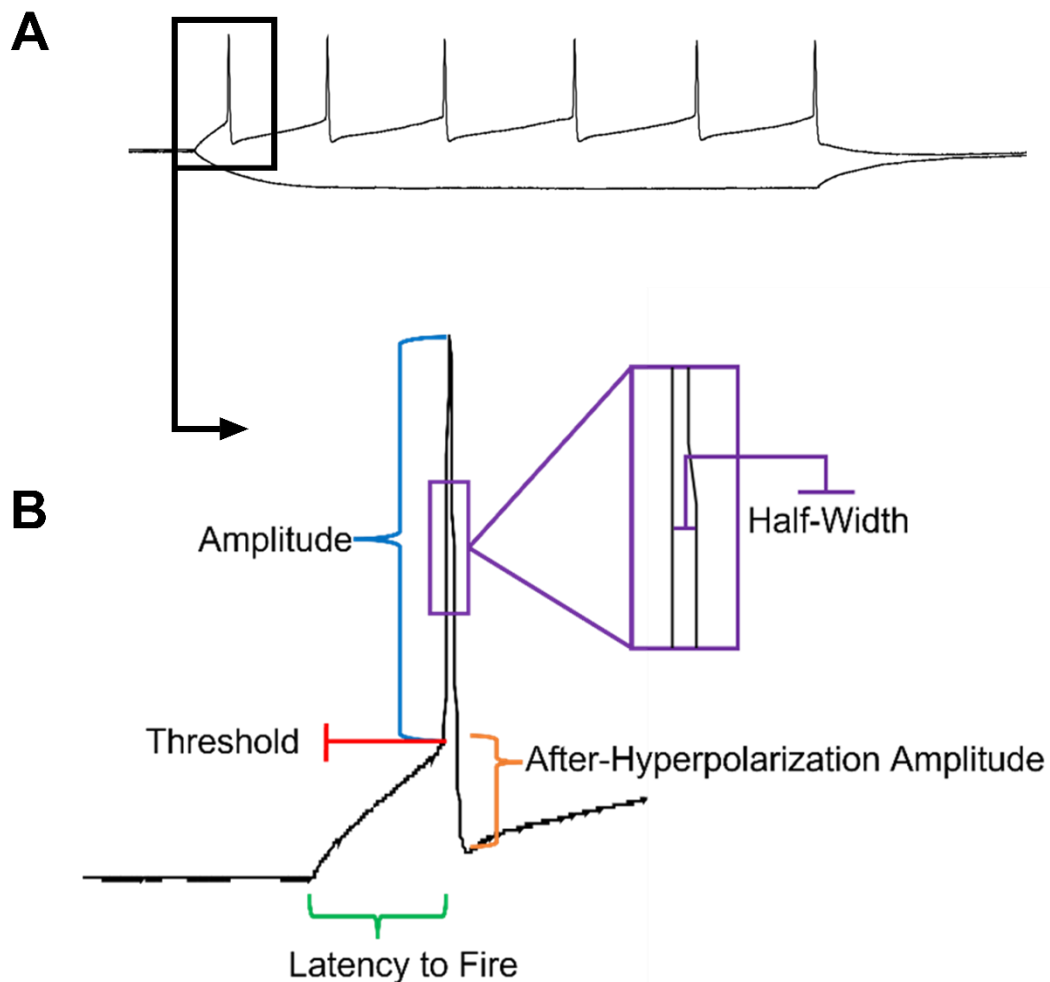


Figure 2.1. Action potential characteristics measured in Clampfit. A) Representative trace of action potential analysis on step one and eight acquired from Clampfit. B) All action potential analyses were performed on the first action potential that was fired once the current clamp protocol was initiated. The threshold value was determined by taking the first derivative of the action potential that occurred first. All subsequent measurements (latency to fire, amplitude, half-width, and after-hyperpolarization amplitude) were measured from the threshold value using Clampfit software.

Evoked synaptic currents were subsequently recorded using voltage clamp mode where the cell was held at -70mV (Figure 2.2). Currents were recorded by positioning the stimulating electrode close to the target neuron to stimulate nearby axons to release neurotransmitter. The resulting currents were recorded from the neuron of interest in the DMH. Once appropriately positioned, the stimulating electrode would evoke two currents at 0.2Hz in 50ms intervals. Two of the evoked excitatory post synaptic currents (eEPSC) were

stimulated every five seconds: current amplitude was measured from the first current, and the ratio of the second to the first current (paired-pulse ratio) was used to assess the probability of release and were used to calculate the paired pulse ratio (PPR) of the second current over the first.

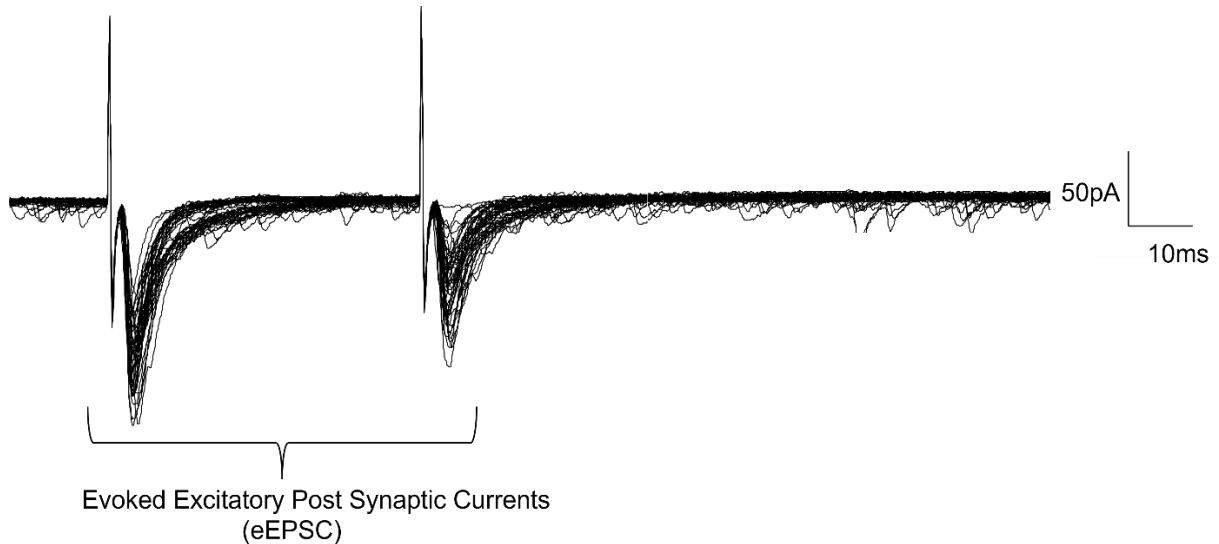


Figure 2.2. Example recording trace of excitatory post synaptic currents. Evoked excitatory post synaptic currents (eEPSC) were stimulated using a stimulating electrode twice every five seconds, at 0.2Hz 50ms apart.

A four-second high frequency stimulation (HFS) protocol was initiated after five minutes of recording baseline evoked currents. During the HFS protocol the stimulating electrode stimulated axons at 100Hz for four seconds, two times, 20 seconds apart. Following HFS, the evoked currents were measured for an additional 25 minutes.

2.4 Experimental Outline for Electrophysiology Experiments

L-phenylalanine (*L*-Phe) (1 mM)⁶¹ in aCSF was added to the recording chamber following five minutes of baseline recordings. Picrotoxin (100 μ M) was in the aCSF throughout the experiment to block GABA_A receptors and isolate glutamate currents. After 10 minutes of recording, *L*-Phe was washed out with aCSF and recording resumed for another 10 minutes (Figure 2.3A). Synaptic plasticity was also assessed by delivering HFS to axons around DMH neurons in the presence of *L*-Phe to determine if *L*-Phe triggers long-lasting changes in synaptic strength (Figure 2.3B)³⁵.

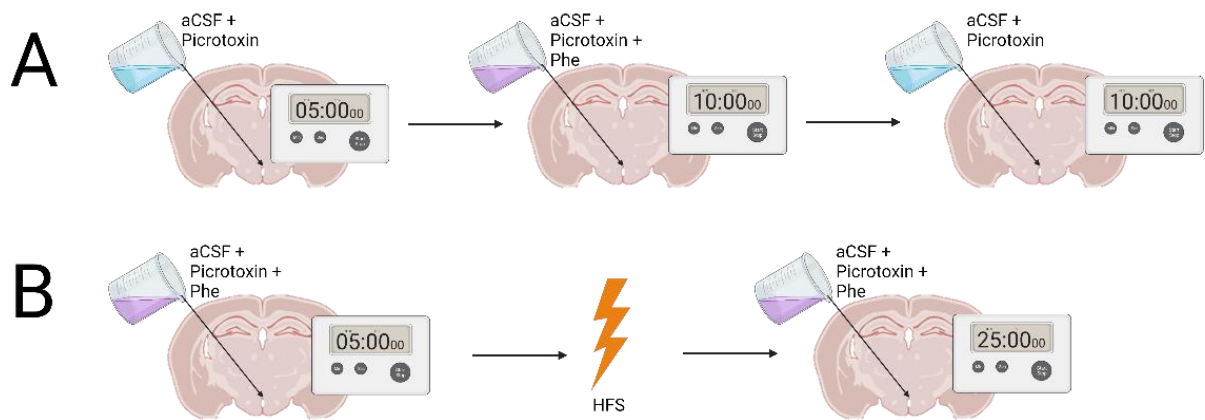


Figure 2.3. Experimental outline of L-phenylalanine experiments. **A)** After 5 minutes of baseline recording with slices incubated in aCSF and picrotoxin, the 1 mM *L*-Phe solution was applied, and recording continued for 10 minutes. The 1 mM *L*-Phe solution was subsequently washed out using aCSF and picrotoxin for another 10 minutes. **B)** High frequency stimulation (HFS) was applied after 5 minutes of baseline recording with aCSF, picrotoxin, and 1 mM *L*-Phe continuously in the recording chamber, followed by cellular recording for an additional 25 minutes.

2.5 Cell Culture

HTLA cells (human modified embryonic kidney cells derived from HEK 293 cells) were obtained from the Roth lab ²¹ and maintained in high glucose (4.5 mg/mL) Dulbecco's Modification Eagles Medium (DMEM, Corning, 10-013-CV) supplemented with 10% Fetal Bovine Serum (FBS, Corning, 35-077-CV) (complete DMEM). To keep the cells in logarithmic growth phase, they were passaged at 70-80% confluency every 48 to 72 hours. Passaging procedure involved washing cells with 1X phosphate buffered saline (PBS), application of 0.25% trypsin/2.21 mM ethylenediaminetetraacetic acid (Corning, 25-053-C1) to detach the cells from the plate, followed by centrifugation at 500 rcf for five minutes. HTLA cells were then resuspended in complete DMEM at a splitting ration of 1:10-1:20. Cells were cultured with puromycin (0.04 μ L/mL, Wisent, 400-160-EM) and hygromycin (2 μ L/mL, Bishop, HYG002.1) to maintain the HTLA stable transgenes.

2.6 Plasmid preparation

Plasmids containing the coding sequences of GPCRs were obtained from the PRESTO-Tango library (Roth Lab, Addgene Kit #1000000068). Standard *E. coli* propagation procedures were used alongside NucleoSpin Plasmid Transfection grade kits for low-yield purification. DNA plasmid concentrations were quantified using Nanodrop spectrum analysis software. pCMV-beta-galactosidase (β -gal), empty vector pBluescriptSK (pBSK), and green fluorescent protein (GFP) plasmids were a gift from C. Sinal (Dalhousie University).

2.7 PRESTO-Tango assay

The Parallel Receptor-ome Expression and Screening via Transcriptional Output (PRESTO-Tango) is a high-throughput approach allowing for identification and quantification of ligands for various GPCRs. The experimental procedure is outlined below (Figure 2.4).

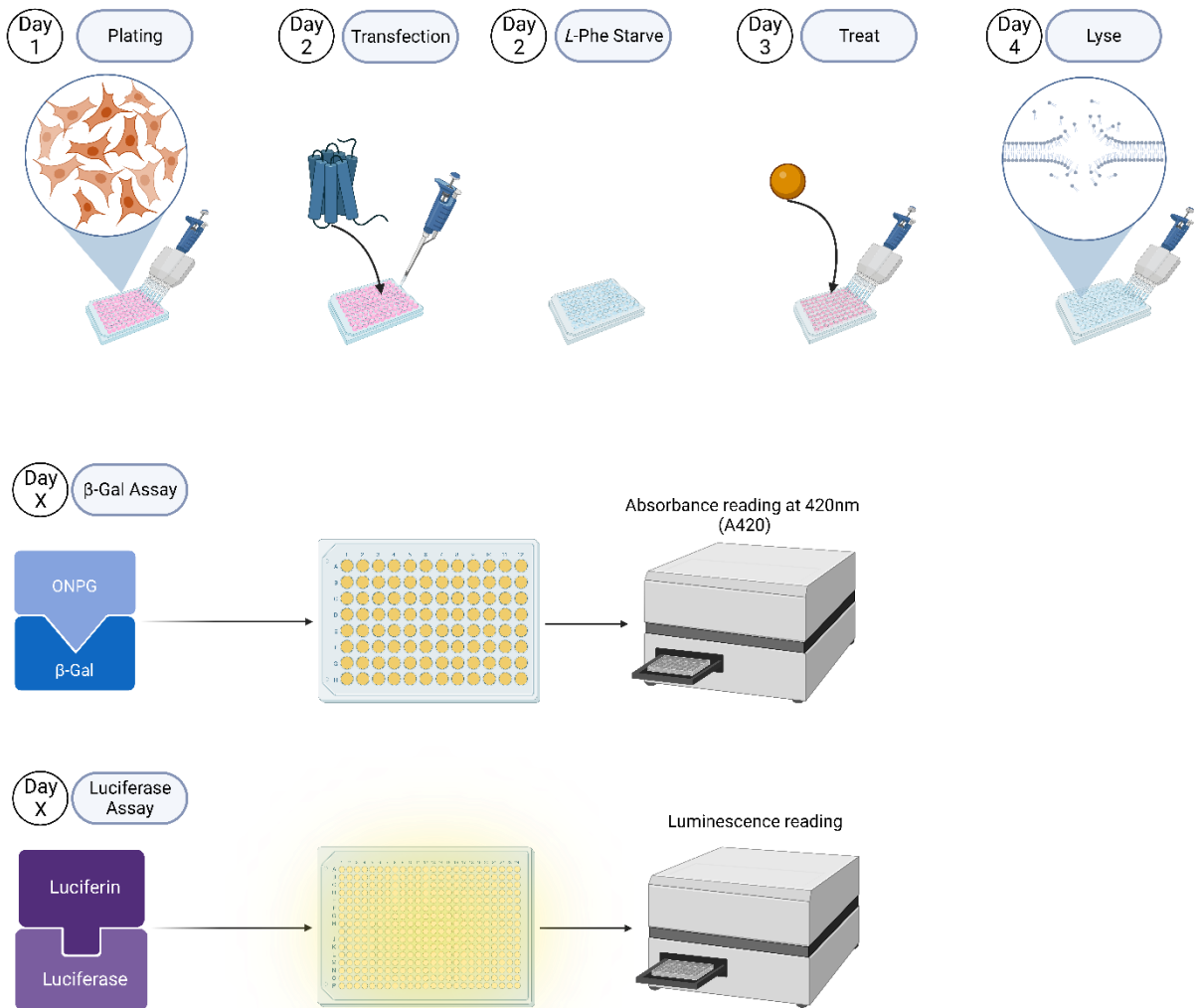


Figure 2.4. Experimental outline of the PRESTO-Tango Assay procedure. Day 1) Plating HTLA cells at 25,000 cells/well in a 96 well plate. Day 2) Cells are transiently transfected with the GPCR plasmid of choice and controls. Day 2) Six hours after transfection, the transfection mix is removed from the cells and replaced with serum free *L-Phe* free DMEM. Day 3) HTLA cells are treated with galanin or *L-Phe*. Day 4) HTLA cells are lysed with 1X firefly reporter lysis buffer and stored at -80°C. Day X) Receptor activity quantified via luciferase and β -gal assays using a BioTek Synergy HT luminescence reader and Gen5 software. Image made using BioRender.

2.7.1 Plating

HTLA cells were washed and lifted off the plate as per passaging procedures. The cells were centrifuged in complete DMEM before being resuspended in serum free DMEM and counted using a hemocytometer. The cells were diluted to 25,000 cells/mL in DMEM containing 5% FBS, plated in a 96-well plate at 100 μ L per well and grown for 24 hours at 37°C at 5% CO₂.

2.7.2 Transfection and *L*-Phenylalanine Starvation

The library of PRESTO-Tango receptor plasmids was obtained from the Roth Lab (Roth Lab, Addgene Kit #1000000068). Plated HTLA cells were transiently transfected with 100 ng of Tango receptor plasmid, 25 ng of a β -galactosidase expressing vector, pCMV- β -gal⁶², 50 ng pBSK (pBluescriptSK,⁶², 0.52 μ L polyethyleneimine (PEI, Sigma Aldrich, 9002-98-6) and 50 μ L Opti-MEM (Reduced Serum Medium, Gibco, 31985-070). 70 μ L of media was removed from the cells and 50 μ L of the transfection mix was added. Transfected cells were incubated at 37°C and 5% CO₂ for six hours after which the media was replaced with 30 μ L of *L*-phe free, serum free DMEM (SF PF DMEM, Wisent, 319-169-CL) and incubated for 18 hours at 37°C and 5% CO₂. Control wells contained, 100 ng pEGFP-N1 (green fluorescent protein, GFP) which acted as a proxy for transfection efficiency and LPAR1 to ensure efficacy of the assay. GFP efficiency was determined using an EVOS microscope (Evos FLC) LPAR1 was additionally transfected as control wells and were treated with either Opti-MEM or 20% FBS which was the negative control, and positive control respectively.

2.7.3 Treatment

Ligands for the GPCRs were diluted to 3X into serum free *L*-Phe free media at the indicated concentrations (appendix, table 1). The pBSK receptor-free transfection controls were treated with Opti-MEM. Cells transfected with LPAR1 were treated with either Opti-MEM (vehicle) or 20% FBS.

Galanin was diluted into TBS (50 mM TRIS buffer (Bishop, 77-86-1) and 150 mM NaCl (Bishop, 7647-14-5), pH 7.4 and filter sterilized) or DMSO (dimethyl sulfoxide, VWR, 67-68-5) then further diluted in serum free *L*-Phe free DMEM to achieve a final 3X concentration.

2.7.4 Cell Lysis

Cells were lysed with 20 μL /well of 1X firefly lysis buffer (Biotium, 3082) in sterile water after removal of all media in the plate. The cells were then agitated for five minutes before being placed in -80°C for a minimum of 24 hours.

2.7.5 Beta gal and Luciferase assay

Once ready for the assay procedure, the plate was removed from -80°C and allowed to thaw at room temperature. To determine β -gal activation, 30 μL of 2X β -gal assay buffer was added to 30 μL of lysate in a fresh 96-well plate. After 10 minutes to allow for a yellow colour to develop, absorbance at 420nm was quantified using a BioTek Synergy HT multiplate reader. The luciferase working solution consisted of 2.5 μL of *D*-luciferin per 100 μL of luciferase assay buffer and 10 μL was added to 20 μL of cell lysate in a 384-well plate. The plate was subsequently covered in aluminum foil and protected from light while being agitated for five minutes before luminescence was quantified using a BioTek Synergy HT luminescence reader. Further it was standardized to RLU/A420 and corrected for background noise using 0.1X lysis buffer as a blank and transformed to fold change by dividing each measurement by the average vehicle measurements.

2.8 MTT Assay

The 3-(4,5-dimethylthiazol-2-yl)-2,5-diphenyltetrazolium bromide (MTT) assay was performed to assess cell viability (figure 2.5). Cells were plated, transfected, and treated as per the PRESTO-Tango assay above. MTT reagent consisted of adding MTT to 1X PBS to a final concentration of 5 mg/mL. 20 hours post treatment, 10 μL of the MTT reagent was added to each well and incubated for 4 hours at $37^{\circ}\text{C} + 5\% \text{CO}_2$ to allow the formation of formazan crystals. The media was then gently removed and 100 μL of DMSO was added to dissolve the formazan crystals. The plate was agitated for 5 minutes before measuring absorbance at 570 nm in the BioTek Synergy HT multiplate reader. Blank values were subtracted prior to calculation of percent viability where Opti-MEM was used as the baseline.

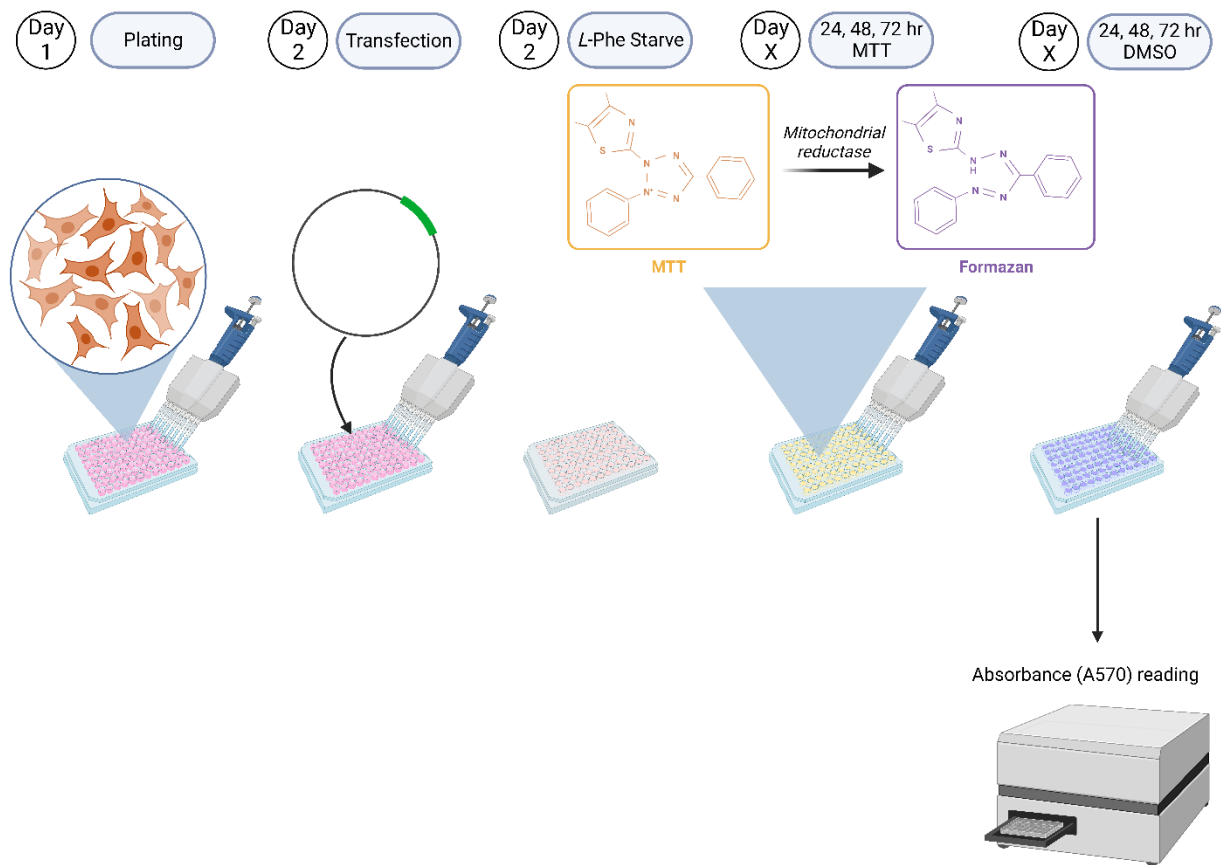


Figure 2.5. Experimental outline of MTT Assay. Day 1) HTLA cells were plated as per the PRESTO-Tango assay above. Day 2) Cells were transiently transfected with the empty plasmid vector pBSK. Day 2) Six hours later, 100% cell media was replaced with *L*-Phe, serum free DMEM. Day X) 20, 44, and 68 hours post *L*-Phe starvation, MTT reagent was added. Day X) Four hours later, DMSO was added to the wells and agitated for five minutes before reading at A570 using a BioTek Synergy HT luminescence reader and Gen5 software. Image made using BioRender.

2.9 Statistical Analysis

To examine glutamate transmission, the amplitude of the first evoked current was averaged for each cell during the 5-minute baseline recording. This was compared to the average evoked amplitude of 10 to 15-minutes of 1 mM *L*-Phe application to ensure that the *L*-Phe was hitting the bath, and 20 to 25-minutes of washout to ensure that the *L*-Phe had been entirely washed out. A repeated measures ANOVA with multiple comparisons was used to compare 1 mM *L*-Phe and washout to baseline recordings and corrected using Tukey multiple comparison testing. If normality or homogeneity of variance did not pass, then the data was

log transformed prior to analysis. The paired pulse ratio (PPR), the ratio of the second evoked current over the first, was averaged for the 5-minute baseline period, and compared to the average PPR for the 10 to 15-minutes of 1 mM *L*-Phe application, and 20 to 25-minute washout period. A one-way ANOVA with multiple comparison testing was used to compare the *L*-Phe and washout PPR, to the baseline PPR, and corrected using Holm-Šídák statistical hypothesis testing.

To examine glutamate mediated currents following high frequency stimulation (HFS), the amplitude of the first evoked current during the 5-minute baseline recording was averaged. The first evoked current was averaged over the 10 to 15-minute period after HFS was applied for all cells. A paired t-test was used to compare the average evoked current of baseline to post-HFS. A paired t-test was also used to compare the post-HFS PPR to the baseline PPR. All time periods reported were chosen to ensure that the *L*-Phe was either hitting the bath or removed.

The mean cell viability of each treatment was compared to Opti-MEM and evaluated using an ordinary one-way ANOVA, corrected using Holm-Šídák statistical hypothesis testing. Dose response curves were fitted with linear regression using log(agonist) vs response. An ordinary one-way ANOVA was performed and corrected using Holm-Šídák multiple comparisons testing was performed comparing each concentration to the vehicle. Galanin receptor activation when treated with DMSO or TBS was evaluated using a one-way ANOVA, corrected using Holm-Šídák multiple comparisons testing. If homogeneity of variance or normality assumptions were not met then the data was log transformed. If the assumptions were not met after transformation, a non-parametric Kruskal-Wallis test was performed.

Statistical analysis and data visualization was performed using Prism 9 (GraphPad software). The significance level for all statistical analysis performed was set at $\alpha = 0.05$.

Chapter 3: Results

3.1 *L-Phenylalanine free media does not alter cell viability*

Vehicle optimization experiments were first performed to ensure that HTLA cells would remain viable in a treatment vehicle that lacked *L*-Phe for use in future experiments. Currently, Opti-MEM is used as a vehicle to treat cells as it doesn't reduce cell viability yet contains high amounts of *L*-Phe that could promote receptor desensitization and interfere with accurate EC50 quantification.

HTLA cells were grown under standard conditions in Opti-MEM for 24 hours and had a corresponding average cellular viability of 112.3%. HTLA viability significantly increased to 167.6% when grown in Dulbecco's Modification Eagle's Medium (DMEM) lacking fetal bovine serum (FBS) (SF) (Opti-MEM: 112.2 +/- 13.76, n = 8; PF with 10% FBS: 130.4 +/- 8.962, n = 9; SF: 167.6 +/- 9.486, n = 8; SF PF: 97.83 +/- 10.56, n = 9; Opti-MEM vs. PF with 10% FBS: Mean rank difference = -5.597, p = 0.999; Opti-MEM vs SF: mean rank difference = -14.94, p = 0.0162; Opti-MEM vs. SF PF: mean rank difference = 2.347, p = 0.999; Figure 3.1A). When the cells were grown in media lacking *L*-Phe supplemented with 10% FBS (PF with 10% FBS) there was no change in cellular viability. Furthermore, there was no significant difference in HTLA cells that were grown for 24 hours in serum free, *L*-Phe free (SF PF) conditions when compared to Opti-MEM.

48 hours after HTLA cells had undergone transfection, there was no significant change in viability when grown in SF compared to Opti-MEM (mean rank difference = -7.444, p = 0.3698). There was a significant increase in HTLA viability when cells were grown in PF (mean rank difference = -17.74, p = 0.0011, Figure 3.1B). There was no difference observed in cells that were grown in SF PF conditions compared to Opti-MEM (mean rank difference = -4.444, p = 0.999, Figure 3.1B). HTLA cells that were grown for 72 hours post transfection in Opti-MEM, SF, PF with 10% FBS and SF PF did not significantly differ in viability between SF and SF PF compared to Opti-MEM (SF vs Opti-MEM: mean difference = 47.67 +/- 37.93, p = 0.3938, Figure 3.1C: SF PF vs Opti-MEM: -30.73 +/- 34.34, p = 0.3938, Figure 3.1C) However, cells grown in PF with 10% FBS experienced, on average, a significant increase in cell viability compared to Opti-MEM (mean difference = -131.7 +/- 34.43, p = 0.0026, Figure 3.1C).

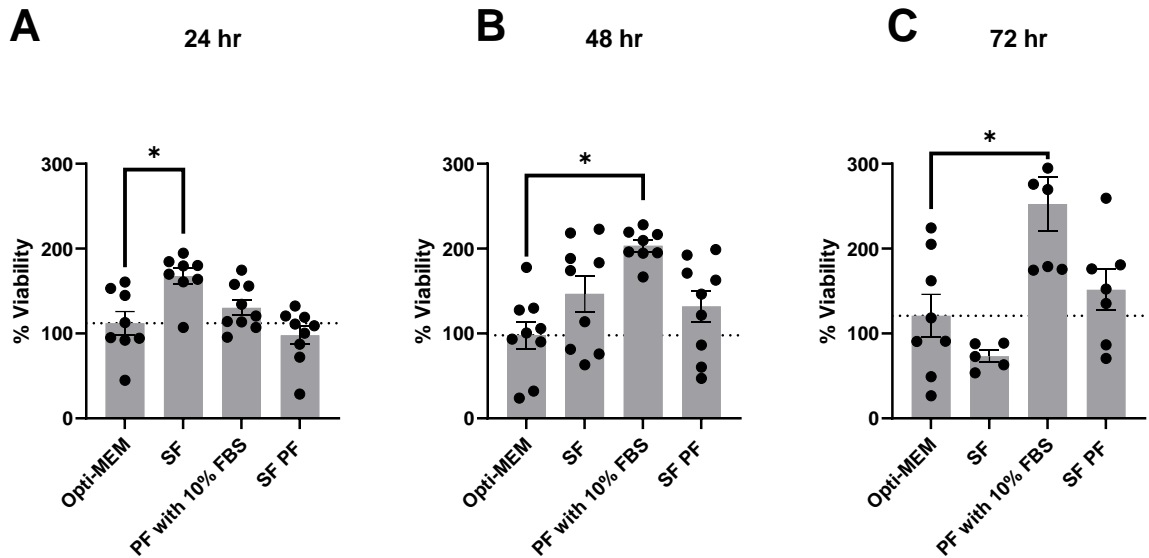


Figure 3.1 *L*-Phe free media does not alter cell viability. HTLA cells transfected with the empty vector plasmid pBSK for 18 hours prior to media exchange to Opti-MEM, DMEM without 10% FBS (SF), *L*-Phe free complete DMEM (PF with 10% FBS), and serum free *L*-Phe free DMEM (PF SF) and remained on for 24 hours (A), 48 hours (B), and 72 hours (C) prior to performing the MTT assay. Dotted lines indicate the average cell viability of Opti-MEM. Data are shown as percent viability compared to Opti-MEM and represented as mean \pm SEM ($n = 3$) and evaluated using a one-way ANOVA, with Holm-Šidák multiple comparisons testing where $\alpha = 0.05$.

3.2 *L*-Phenylalanine dose dependently activates galanin receptor type one

The galanin receptor family members GALR1 and GALR2 contribute to the regulation of energy metabolism and are known to be prevalent in the central nervous system^{63,64}. Determining a concentration dependent relationship with *L*-Phe and galanin receptors is crucial to understanding the biological relevance of *L*-Phe activation and galanin receptors. HTLA cells were transiently transfected with GALR1 or GALR2 as per the PRESTO-Tango procedure and treated with *L*-Phe or galanin in medium lacking in *L*-Phe free.

L-Phe activated GALR1 in a concentration-dependent manner resulting in an EC50 of 754.5 μ M (Figure 3.2A). A significant increase in GALR1 activation occurred when HTLA cells were treated with *L*-Phe concentrations exceeding 250 μ M. The same effect was not observed with HTLA cells transfected with GALR2 (figure 3.2B). A significant fold change activation did occur when cells expressing GALR2 were treated with 5,000 μ M *L*-Phe compared to vehicle treatment.

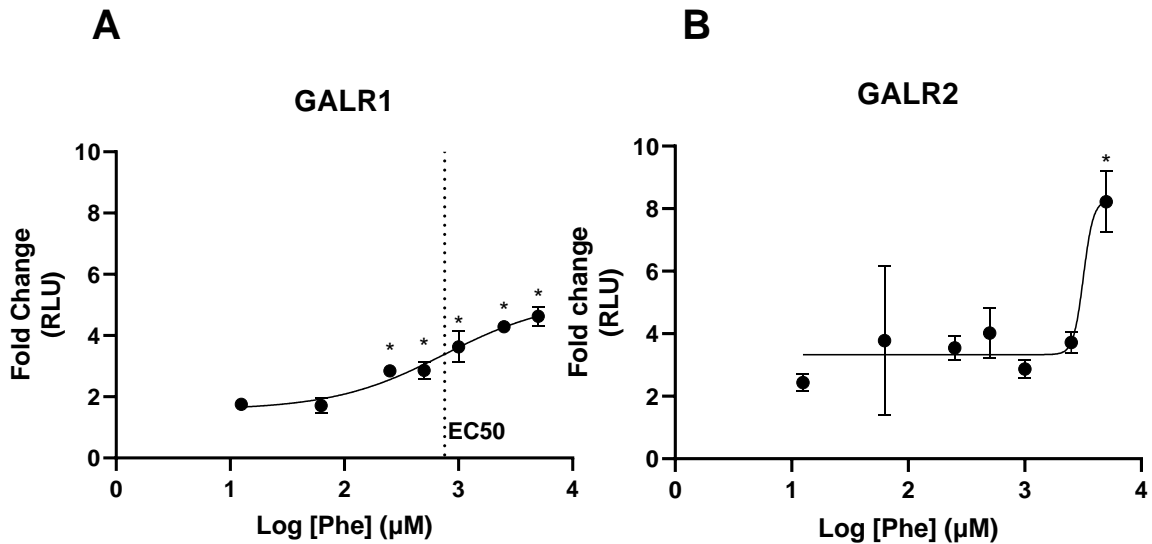


Figure 3.2. *L*-Phe dose dependently activates galanin receptor type one. HTLA cells were treated with *L*-phe (0 μ M to 5,000 μ M) following transfection of galanin receptor type 1 (A) or type 2 (B). Dotted line indicates logEC50 value of 2.878 (EC50 = 754.4 μ M). The luciferase/ β -galactosidase activity (relative light units (RLU)) was determined and expressed relative to the vehicle as fold change and corrected using the blank luminescence. Data are represented as mean \pm SEM (n=1) and curves were fitted with linear regression using log(agonist) vs response. One-way ANOVA corrected using Holm-Šídák multiple comparisons testing where $\alpha = 0.05$.

Galanin treatment (0 μM to 3 μM) of HTLA cells expressing GALR1 or GALR2 did not result in any receptor activation (Figure 3.3A, B). The lack of receptor activation was unlikely to be an issue with receptor expression as there was strong green fluorescent protein (GFP) levels indicative of adequate transfection efficiency (Figure 3.4A, B). Therefore, the inability for GALR1 and GALR2 to signal *via* the PRESTO-Tango assay is likely because of the galanin peptide or the diluent used.

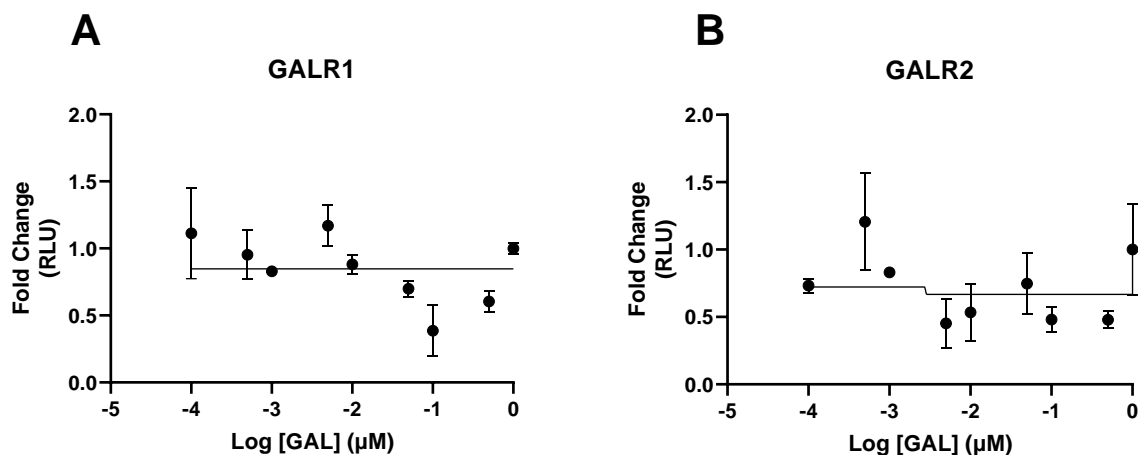


Figure 3.3. Galanin treatment did not activate receptor type one and two. HTLA cells (HEK 293 A derived cells expressing tTA-dependent firefly luciferase reporter gene and a β -arrestin2-TEV fusion gene) were treated with galanin (0 μM to 3 μM) following transfection of GALR1 (A) and GALR2 (B). The luciferase/ β -galactosidase activity (relative light units (RLU)) was determined and expressed relative to the vehicle as fold change and corrected for using the blank luminescence. Data are represented as mean \pm SEM (n=1) and the curves were fitted with linear regression using log(agonist) vs response.

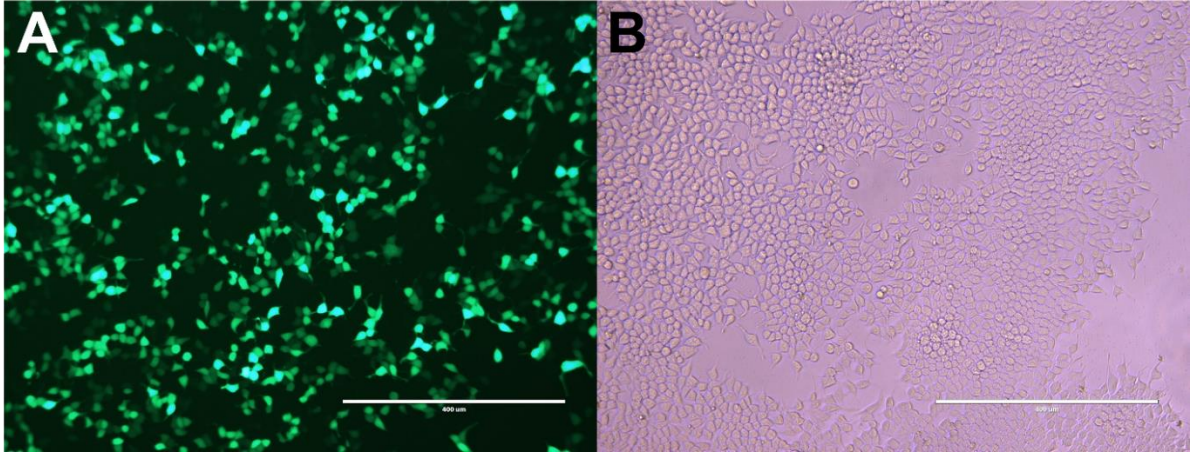


Figure 3.4. HTLA cells expressing green fluorescent protein (GFP). (A) Green fluorescent protein (GFP) expression in HTLA cells. (B) Transmitted light image of HTLA cells transfected with GFP. Images obtained using EVOS microscope, scale bar of 400 μm .

3.3 Galanin in TBS or DMSO activates GALR1 and GALR2

The inability for GALR1 and GALR2 to be activated in the concentration response curve (CRC) could have been attributed to the diluent used. Therefore, the need to optimize the diluent was important for future steps. HTLA cells were transfected with GPCR plasmids encoding for GALR1 or GALR2 and treated with galanin dissolved in TBS or DMSO^{65,66} (dimethyl sulfoxide) diluted in serum free *L*-Phe free DMEM at 0 μ M, 1 μ M, or 10 μ M.

Transfection with either GALR1 or GALR2 showed a trend to increase basal luciferase (Opti-MEM) consistent with successful receptor expression and a low level of constitutive receptor signaling. There was no significant difference in activation of GALR1 for galanin dissolved in either TBS or DMSO at low (1 μ M) or high (10 μ M) concentrations compared to vehicle treatments (0 μ M GAL) (appendix, table 3, Figure 3.5A). Triplicates from one biological replicate showed a strong upward trend when treated with galanin. This effect was not reproduced in the two subsequent biological replicates. The same trends were observed for GALR2 (appendix, table 4, Figure 3.5B)

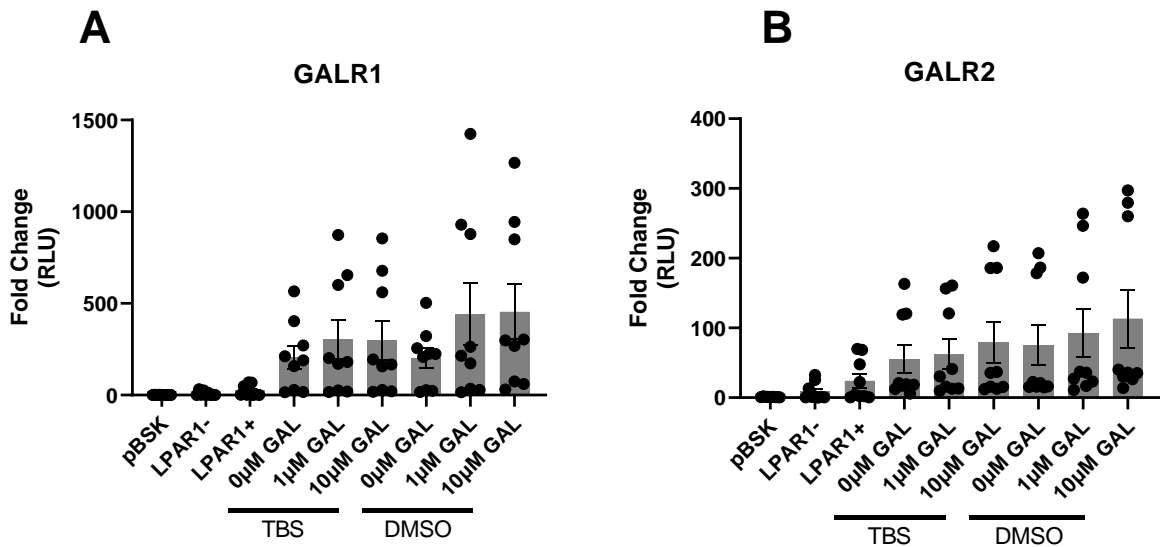


Figure 3.5. Galanin receptors are activated by galanin dissolved in TBS or DMSO. HTLA cells were transfected with galanin receptor family type 1 (A) or type 2 (B) and treated with galanin dissolved in TBS or DMSO at 0 μ M, 1 μ M and 10 μ M. Luciferase/b-galactosidase activity (relative light units (RLU)) was determined and expressed relative to the vehicle as fold change. Data represented as mean \pm SEM (n = 3) and evaluated using a one-way ANOVA, corrected using Holm-Šidák multiple comparisons testing where $\alpha = 0.05$.

3.4 *L*-Phenylalanine reduces glutamate transmission in the DMH of male rats

The DMH is an ideal brain region to study the effects of *L*-Phe. Neurons in the DMH are important in appetite regulation and *L*-Phe has been reported to trigger satiety^{44,48,67}. In addition, receptors known to respond to *L*-Phe are expressed in the DMH⁶⁴. Understanding the effect of *L*-Phe on neurons could improve our understanding as to how *L*-Phe affects satiety. Because DMH neurons are known to stimulate hunger, it is possible that *L*-Phe suppresses the activity of these neurons, an effect that could be achieved by decreasing glutamate signaling in the DMH. Consistent with this idea, it has previously been found that cultured neurons from the hippocampus and cerebro-cortical region display a decrease in glutamate transmission. To elucidate the effect of *L*-Phe on glutamate transmission in the DMH, a 1 mM *L*-Phe solution was applied to living brain slices containing DMH neurons. Whole cell patch clamp electrophysiology was performed to observe changes in glutamate current amplitude by blocking GABA_A receptors.

The amplitude of glutamate currents was significantly decreased when *L*-Phe was added to DMH neurons compared to baseline (92.271 ± 0.8021% baseline, $p < 0.0001$, $n = 11$, Figure 3.6B). Additionally, a significant decrease in current amplitude was observed in washout compared to baseline current amplitude (86.79 ± 0.8021% baseline, $p < 0.0001$, $n = 11$, Figure 3.6B). The paired-pulse ratio was next determined to assess whether the above changes were due to a decrease in the probability of release of glutamate (PPR is inversely proportional to release probability). There was no significant difference in the PPR between baseline, 1mM *L*-Phe, and washout measurements (baseline: 1.344 ± 0.1461, $n = 12$; *L*-Phe: 1.184 ± 0.7781, $n = 11$; washout: 1.216 ± 0.1278, $n = 10$; baseline vs. *L*-Phe: mean difference = 0.1605 ± 0.2451, $p = 0.8877$; baseline vs washout: mean difference = 0.1287 ± 0.2514, $p = 0.8877$, Figure 3.6C) indicating no change in the probability of neurotransmitter release when *L*-Phe is present or washed out when compared to baseline indicating that intracellular calcium levels are not reaching threshold levels to promote the release of neurotransmitters.

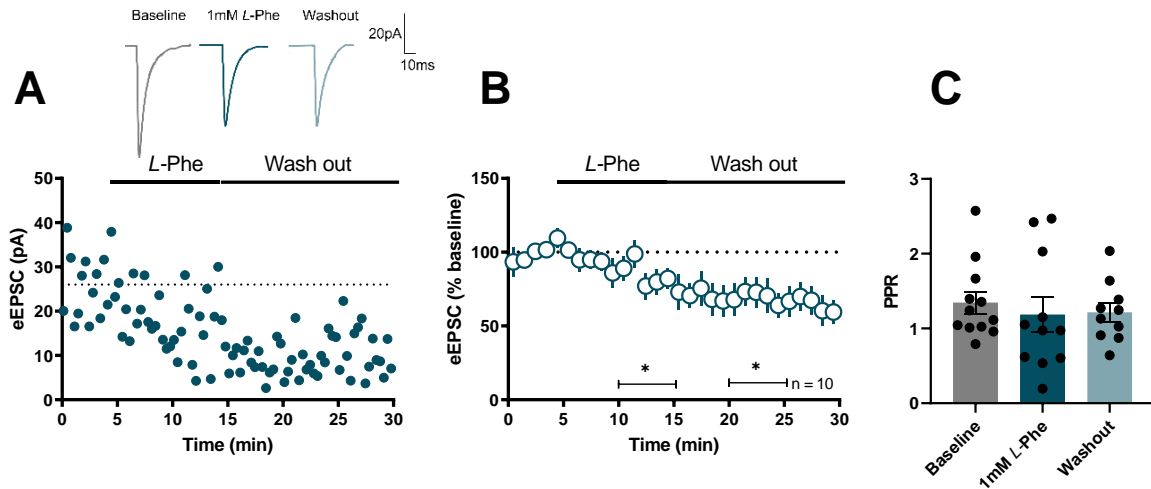


Figure 3.6. *L*-Phenylalanine decreases glutamate transmission in the dorsomedial hypothalamus. **A)** Representative cell depicting evoked excitatory post synaptic currents (eEPSC) in picoamps (pA) over time (min) at baseline (0-5 min), 1mM *L*-Phe application (5-15 min) and subsequent wash out (15-30 min). Data represented as mean \pm SEM and the dotted line indicates the average baseline amplitude. **B)** Summary data illustrating eEPSC amplitude normalized to baseline, with the addition of 1mM *L*-Phe, and washout with aCSF and picrotoxin. The dotted line represents the average baseline amplitude. **C)** Paired pulse ratio (PPR) comparison between baseline, 1mM *L*-Phe, and washout. Data evaluated using a repeated measures ANOVA comparing baseline (0-5 minutes) to 1mM *L*-Phe (10-15 minutes) and washout (20-25 minutes), corrected for using Tukey multiple comparisons testing where $\alpha = 0.05$.

3.5 *L*-Phenylalanine does not significantly alter neuronal excitability at neurons in the DMH

To determine the effect of *L*-Phe on neuronal excitability, neurons were sequentially depolarized using the current clamp protocol. When the current clamp protocol was initiated, the stimulating electrode incrementally injected current to depolarize the cell from approximately -100 mV to -10 mV. Action potential frequency was measured at each step and the first derivative of the first occurring action potential was taken to achieve information about the threshold. The peak amplitude, half-width, and after hyper polarization amplitude were subsequently measured from the threshold value.

In naïve animals, there was an increase in action potential firing at increasing injected currents as was expected. A similar trend was observed when *L*-Phe was applied to the brain slice, however there was a significant decrease in the frequency of fired action potentials when compared to baseline (mean difference = 5.471 +/- 2.13, $p = 0.0293$, Figure 3.7A). Additionally, there was a significant decrease in the frequency of action potentials in the washout group compared to baseline (mean difference = 6.736 +/- 2.380, $p = 0.0228$, Figure 3.7A), and no significant change in *L*-Phe addition, and washout groups (mean difference = 1.265 +/- 2.477, $p = 0.6128$, Figure 3.7A).

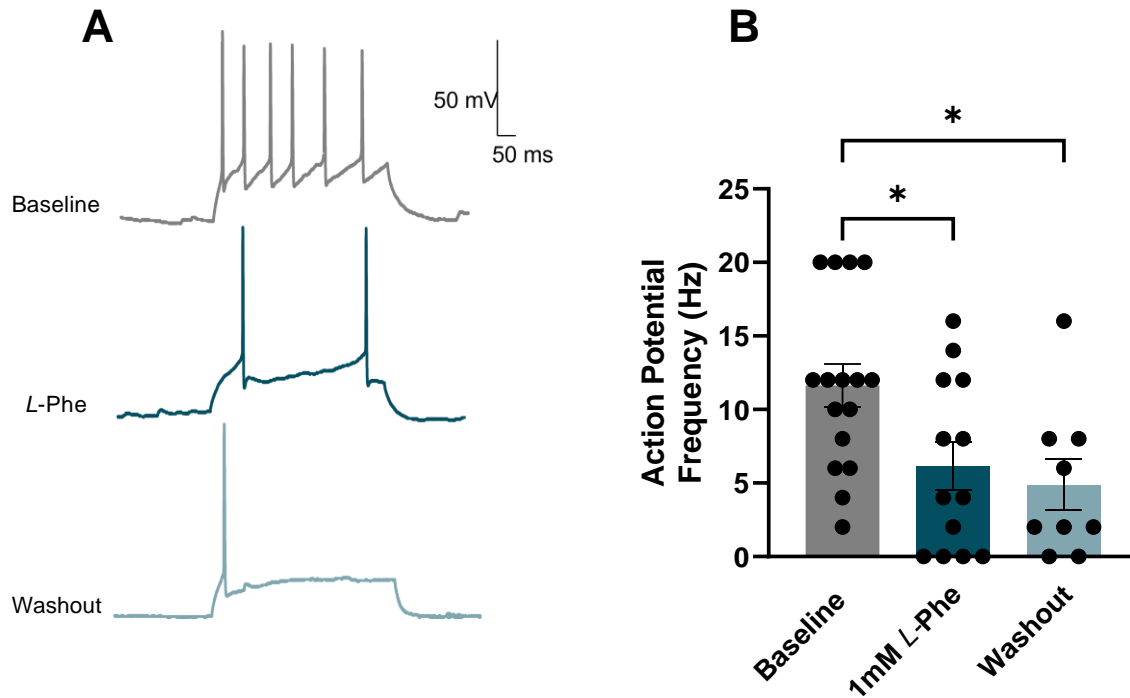


Figure 3.7. *L*-Phe significantly decreases neuronal excitability in the DMH. (A)

Representative action potential traces at an injected current of -30 mV (corresponding to step eight of ten of the current clamp steps protocol) and -100 mV (corresponding to step one of ten). **(B)** Frequency of action potentials fired at an injected current of -30 mV. Data represented as mean \pm SEM for each of baseline, 1 mM *L*-Phe application, and subsequent washout.

We additionally measured other intrinsic properties of action potentials. A significant decrease in the latency to fire of action potentials compared to baseline when both 1mM *L*-Phe (mean difference = 61.57 ± 24.03 , $p = 0.0295$), and washout (mean difference = 85.18 ± 28.43 , $p = 0.0149$) occurred (Figure 3.8A). There was no significant difference in other properties of action potentials such as threshold (baseline vs. *L*-Phe: mean difference = 1.935 ± 2.337 , $p = 0.7983$; baseline vs. washout: mean difference = 1.915 ± 2.710 , $p = 0.7983$, Figure 3.8B), peak amplitude (baseline vs. *L*-Phe: mean rank difference = 5.938 , $p = 0.4254$; baseline vs. washout: mean rank difference = 1.625 , $p = 0.99$, Figure 3.8C), half-width (baseline vs. *L*-Phe: mean difference = -0.07979 ± 0.1963 , $p = 0.7191$; baseline vs. washout: mean difference = 0.1663 ± 0.2276 , $p = 0.7191$, Figure 3.8D) or after hyperpolarization amplitude (baseline vs. *L*-Phe: mean difference = 0.6398 ± 1.944 , $p = 0.8162$; baseline vs. washout: mean difference = -1.257 ± 2.198 , $p = 0.8162$, Figure 3.8E) in *L*-Phe or washout when compared to baseline.

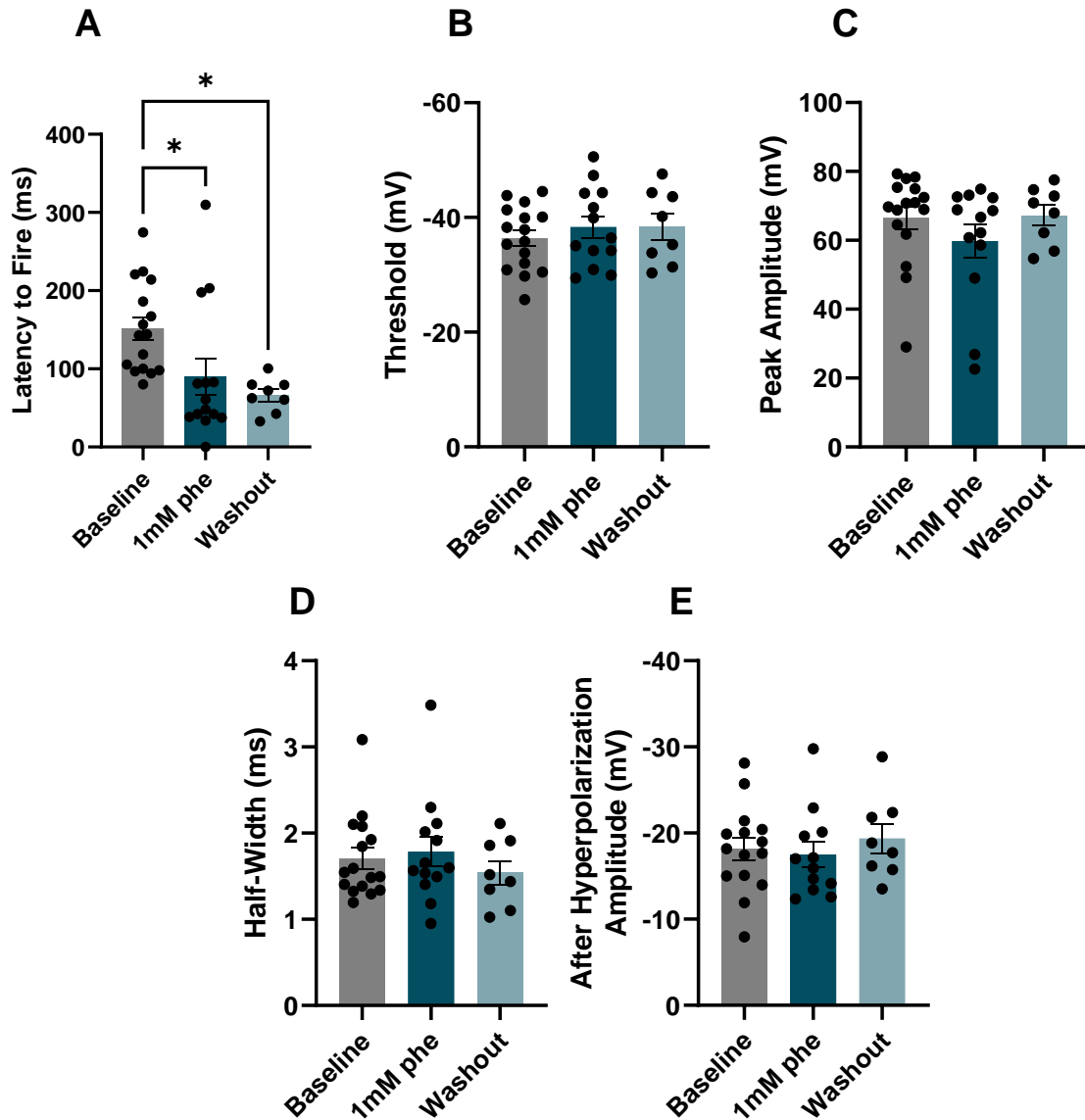


Figure 3.8. *L*-Phe decreases latency to fire but does not alter alternative properties of action potentials. (A) A significant decrease in the latency to fire was observed in 1mM *L*-Phe and washout when compared to the baseline conditions. The (B) threshold was determined from the first derivative of the first action potential fired when current clamp steps protocol was initiated. The (C) peak amplitude (D) half-width, and (E) after hyperpolarization amplitude were all obtained from the threshold value, and there was no significant difference noted in these values.

3.6 A long term decrease in synaptic strength occurs as a result of L-Phe

Aberrant increases of *L*-Phe concentration in the brain is most often seen in classical cases of phenylketonuria (PKU). It is possible that prolonged elevations in *L*-Phe, as seen in PKU, can trigger long-lasting changes in synaptic strength.. After five minutes of baseline current recordings, a four-second-high frequency stimulation (HFS) protocol was delivered to examine whether synapses in the DMH undergo long-lasting changes in strength in the presence of *L*-Phe. This protocol consists of two, four second 100Hz bursts of stimulation occurring at 20 second intervals. A long-term potentiation (LTP) refers to an increase in synaptic strength, while a long-term depression (LTD) refers to a decrease in synaptic strength.

Alterations in synaptic strength were investigated by comparing the baseline current amplitude (0-5 minutes) to post-HFS current amplitude (20-25 minutes). In control animals, there was no difference in the evoked currents following HFS compared to baseline (100.8 +/- 32.4 % of baseline, n = 9, p = 0.7214, Figure 3.9B). In the presence of 1mM *L*-Phe present, there was a significant decrease in the eEPSC amplitude following HFS when compared to baseline (75.00 +/- 6.679 %baseline, p = 0.0025, n = 15, Figure 3.9E). A significant decrease of eEPSC amplitude in the presence of 1mM *L*-Phe (Figure 3.9E) when compared to control (Figure 3.9B) indicates that *L*-Phe is the likely factor responsible for the decrease in synaptic strength of neurons in the DMH.

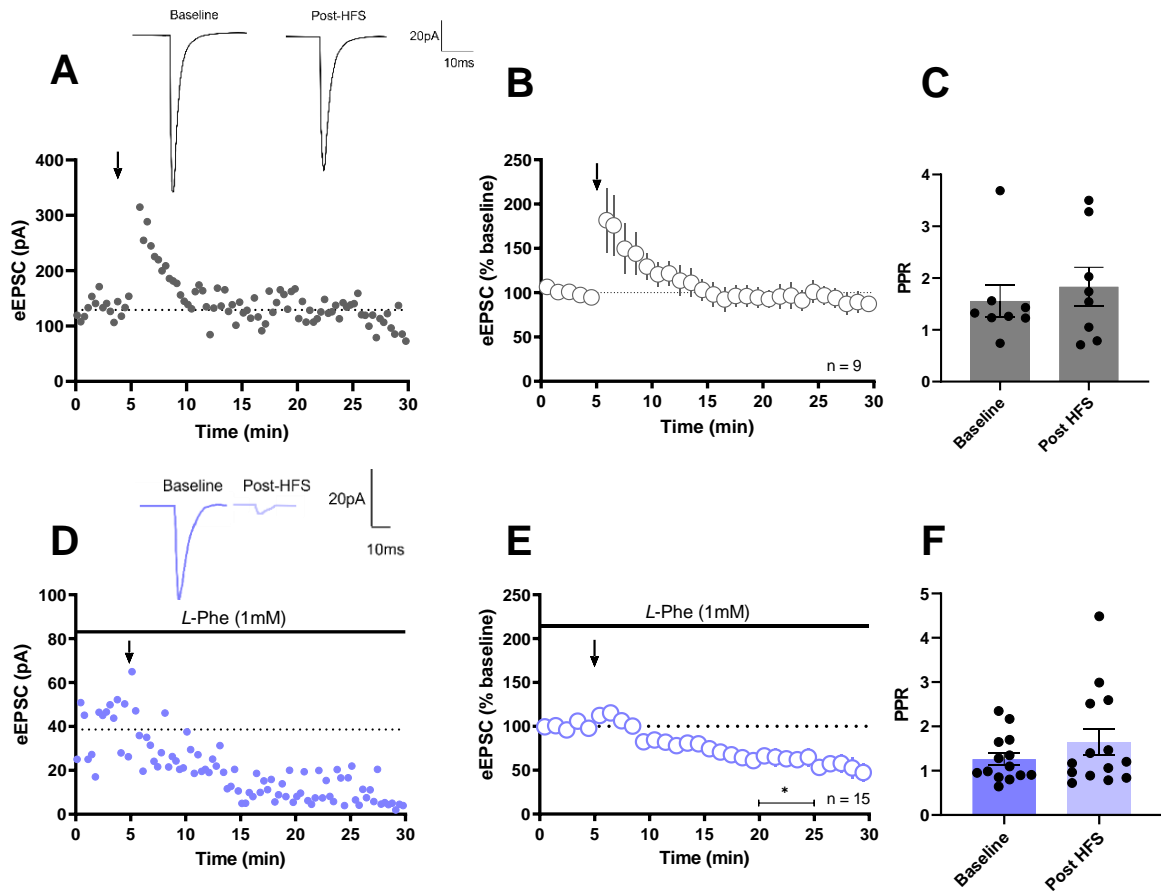


Figure 3.9. Glutamate synapses undergo long-term depression following HFS in the presence of *L*-Phe. (A) Evoked excitatory post synaptic currents (eEPSC) of a representative control cell that has undergone high frequency stimulation (HFS) indicated by an arrow. (B) Summary of all recorded control cells showing the percent change in amplitude of eEPSC over time. (C) Paired pulse ratio (PPR) comparisons between baseline and post-HFS of control data. All control data was collected by Tenea Welsh. (D) Representative cell that has undergone high frequency stimulation (HFS) indicated by an arrow, in the presence of *L*-Phe. Illustrated above the graph are representative evoked excitatory traces. Dotted line indicates average baseline current amplitude in picoamps (pA). (E) Graphs depicting the eEPSC as a percent change from baseline of cells that underwent HFS, indicated by an arrow in the presence of *L*-Phe. (F) Paired pulse ratio (PPR) comparisons between baseline and post HFS in the presence of *L*-Phe. Dotted line indicates average baseline current amplitude in picoamps (pA).

We have displayed shown that HTLA cells do not alter in viability when exposed to *L*-Phe free media. Additionally, *L*-Phe activates GALR1 in a dose dependent manner resulting in an EC50 of 754.4 μ M and therefore is a *bone fide* *L*-Phe receptor. However, GALR2 is not dose dependently activated. We have also shown that GALR1 and GALR2 are not preferentially activated when galanin is dissolved in TBS or DMSO indicating that either vehicle is appropriate for dissolution and storage of galanin. Finally, *L*-Phe is able to decrease neuronal activity in the DMH by reducing glutamate transmission, inducing a long-term decrease in synaptic strength of neurons, as well as decrease action potential frequency.

Chapter 4: Discussion

L-Phenylalanine (*L*-Phe) is well known as a protein building block, and neurotransmitter precursor. However, the effects of *L*-Phe on the dorsomedial hypothalamus (DMH), and subsequent G protein-coupled receptor (GPCR) activation has not been well explored. We have displayed compelling evidence that *L*-Phe dose dependently activates galanin receptor type 1 resulting in an EC50 of 754.4 μ M. Additionally, 1 mM *L*-Phe causes a decrease in neuronal excitability, glutamate transmission, and a long-lasting decrease in synaptic strength.

L-Phe is an important protein building block and has been recently found by the Rourke lab to activate several class A neuronal G protein-coupled receptors (GPCRs) (Figure 1). *L*-Phe is known to activate a wide range of GPCRs, however, a concentration dependent relationship between several class A GPCRs and *L*-Phe has not been explored, specifically, the galanin receptor family (GALR1, GALR2, and GALR3). Here, we present findings on HTLA cell viability in *L*-Phe free media as well as galanin diluted in TBS or DMSO activating GALR1 and GALR2. Moreover, we show that *L*-Phe activates GALR1-expressing HTLA cells in a concentration-dependent manner, indicating that GALR1 could be a *bone fide* *L*-Phe receptor.

Opti-MEM is a serum reduced media that is almost universally used in transfection procedures to dilute the DNA plasmid to be introduced to the cell ^{21,69}. Media lacking *L*-Phe had been previously used on HTLA cells to assess receptor activation without additional *L*-Phe present ⁷⁰. However, it is unclear if media lacking *L*-Phe disrupts the viability of these cells. Our results indicate that HTLA cells do not have significant alterations in cell viability when *L*-Phe is not present, compared to HTLA cells in Opti-MEM suggesting *L*-Phe is a suitable replacement for Opti-MEM as a vehicle treatment for HTLA cells. It is important to note that previous findings indicated that cell growth media containing various concentrations of selective amino acids did not significantly reduce mammalian cellular viability ⁷¹. However, *L*-Phe was not one of the selected amino acids and therefore could differ from the stated results. It is pertinent moving forward to understand how amino acid deficient growth media impacts metabolic activity of cells as it could help indicate various pharmacological therapeutics and help to direct biotechnological advancements.

Following confirmation that *L*-Phe-free, serum-free media is a suitable vehicle replacement for Opti-MEM, we were able to characterize a concentration dependent response of GALR1 and *L*-Phe. This is consistent with previous findings stating that calcium sensing receptors (CaSR) are dose dependently activated by *L*-Phe⁷². Wang et al., (2006)⁷² identified an EC50 of 299 +/- 36 μ M *L*-Phe for CaSR, while we determined an EC50 value of 754.4 μ M for GALR1. However, the reported EC50 for galanin binding to GALR1 was 1.1 nM which is a 200% difference in EC50 values⁷³. This would indicate that *L*-Phe has an increased binding affinity for GALR1 than galanin, however, ligand binding assays and computational simulations would need to be performed to confirm this. Variation in EC50 values is likely attributed to the different receptors used and the variation in binding affinity for *L*-Phe. It is however important to note that *L*-Phe is able to activate GALR1 in a dose-dependent manner. This finding furthers our understanding of the link between this receptor and *L*-Phe and could contribute to pharmacological advancements. Phenylketonuria (PKU) is classified as serum *L*-Phe levels persistently greater than 120 μ M, and becoming dangerous at levels exceeding 1,200 μ M⁷⁴. The EC50 we had identified fits comfortably in this range and would likely be better attributed to the pathogenesis of PKU.

Initially, galanin had been dissolved in TBS as this diluent had previously been used to activate both GALR1 and GALR2 in a concentration dependent manner⁶⁵. Our results were inconsistent with these findings as we did not achieve a concentration response curve for GALR1 or GALR2 treated with galanin leading us to perform a series of troubleshooting assays to optimize the diluent. Diluent optimization was a necessary first step for three main reasons; 1) neither receptor was activated by galanin, 2) there was adequate GFP expression indicating successful transfection of plasmids, and 3) both receptors were activated by *L*-Phe indicating sufficient treatment procedures. Consistent freezing and thawing of peptides has been shown to cause instabilities with the pH of the peptide and of the buffered solution, and could therefore provoke denaturation of the protein and a reduction in function⁷⁵. This could have occurred while preparing the galanin treatment as galanin was frequently thawed and refrozen. Dose dependent activation of GALR1 and GALR2 has been shown when galanin is dissolved in dimethyl sulfoxide (DMSO)⁶⁶ and therefore could pose as an alternative diluent to TBS for activation of these receptors.

The need to determine activation of GALR1 and GALR2 when treated with galanin dissolved in TBS and DMSO was vital as it could indicate a preferential vehicle for galanin dissolution and storage. When comparing the activation of GALR1 and GALR2 of galanin dissolved in TBS or DMSO, there was no significant difference in receptor activation between either vehicle treatments, or between 1 μ M and 10 μ M concentrations. There was however a strong upward trend in one of the biological triplicates likely that was not seen in subsequent experiments. This strong upward trend is likely increasing the mean and therefore causing a lack of significance.

This is consistent with previous dose response curves indicating that the galanin receptors are activated when treated with galanin dissolved in TBS or DMSO^{65,66}. However, this proved inconsistent with the dose response curves presented here as the receptors lacked activation when treated with galanin in TBS. These results are therefore inconclusive as an increase in galanin receptor activation was observed when optimizing the diluents but was not seen in the concentration response curve. Future studies could explore receptor localization on the cellular membrane as well as using fresh galanin for treatments to reduce the effects of consistent freezing and thawing.

The dorsomedial hypothalamus (DMH) is a brain region containing neurons that stimulate hunger, but the control of these neurons is not fully understood. Dietary nutrients, including glucose, can affect the release of neurotransmitters, such as glutamate, in the brain, but the effect of proteins/amino acids are less well known. *L*-Phe is an important dietary amino acid that binds to receptors expressed in the DMH, but nothing is known about how Phe affects glutamate transmission in the DMH. The effect of *L*-Phe has been explored in the hippocampus and cerebellum and results indicate that *L*-Phe depresses glutamate transmission⁶¹, however its effects have not yet been explored in the dorsomedial hypothalamus. We performed whole cell patch clamp electrophysiology on living neurons in the DMH in the presence of 1 mM *L*-Phe to observe changes in neuronal activity, synaptic transmission, and long-lasting changes in synaptic strength.

Action potentials provide information on intrinsic properties of neuronal excitability. We examined the effect of *L*-Phe on action potential firing and found that there is a decrease in the frequency of action potentials when compared to baseline. Additionally, there was a decrease in the latency to fire when *L*-Phe was present compared to baseline. To the best of our knowledge, this is the first study indicating the effect of *L*-Phe on the frequency of action potentials. Neuronal excitability has been found to be decreased when galanin receptors are activated. Galanin binding to galanin receptors opens K^+ channels and allows the cell to hyperpolarize, therefore making it less likely to fire an action potential ⁷⁶. *L*-Phe could be initiating a similar response corresponding to a decrease in neuronal excitability. This is in concert with another study that found that application of aspartate decreased action potential firing in mongrel cats ⁷⁷. A decrease in action potential firing could influence the release of neurotransmitters across the synapse. When *L*-Phe was present, there was no significant change in the probability of release of neurotransmitter. A significant difference could occur if *L*-Phe remained in the bath for longer than the performed 10 minutes. Future studies could examine chronic exposure of *L*-Phe to assess any potential differences that may be occurring beyond a 10-minute application.

Application of *L*-Phe reduces glutamate transmission in the DMH and was not reversible upon washout. This could be due to *L*-Phe binding, and competing for the glycine binding site of NMDA receptors ⁶¹. *L*-Phe antagonizes both NMDA and AMPA receptors upon binding and would therefore inhibit glutamate binding. Our data indicates a depression in glutamate mediated currents in the dorsomedial hypothalamus, while Glushakov et al., (2003) noted a similar depression in glutamate currents in the hippocampus. *L*-Phe could mediate this affect through competitive binding on the glycine-binding site of the NMDA receptors, and inhibiting glutamate binding ⁷⁸. The DMH is known for its ability to increase appetite in response to an increase in glutamate signalling ^{49,67}. Therefore, a decrease in glutamate transmission, as a result of *L*-Phe, could ultimately decrease appetite in young male rats. Future work should examine the effects in female animals when exposed to *L*-Phe to determine a potential sex-based difference. It is possible that there will be a sex-based difference on glutamate mediated currents in response to *L*-Phe because of the pre-established difference in food intake in males and females. Additionally, there are well established sex based differences observed in individuals with phenylketonuria such that females tend to

exhibit more severe symptoms than males^{79,80}. It is unlikely that GABA synapses would be affected *L*-Phe administration as it has been previously determined that the expression of the GABA_A receptor $\alpha 1$ subunit was neither increased nor decreased in mice with PKU⁶¹, and therefore is not likely to play a role in pathology of PKU in the DMH. Future work should aim to inhibit GPCRs in the brain and reinvestigate the effect of 1 mM *L*-Phe to determine if the observed affect could be additionally mediated by GPCRs. This could be accomplished by introducing GTP β -S, a GPCR inhibitor, into the recording electrode to inhibit the recruitment of G-proteins to the GPCR and therefore inhibit signaling⁸¹.

Here we report that *L*-Phe induces a long-term depression (LTD) of plasticity at glutamate synapses in male rats. This could be due to a decrease in dendritic spine formation which is known to occur in chronic, untreated cases of phenylketonuria⁸². Therefore, increased *L*-Phe concentrations could cause a decrease in neuronal activity *via* a decrease in dendritic spines. To determine whether LTD is presynaptic or postsynaptic in nature we examined the paired pulse ratio (PPR). There was no significant change in the PPR and therefore we can not confidently conclude the locus of the LTD. However, there is an indication that the PPR is increasing and could correlate to the observed LTD likely being postsynaptic in nature^{83,84}. Confirmation would be required by assessing the spontaneous excitatory current amplitude and frequency. If the frequency of spontaneous currents are unchanged then it is more likely the observed LTD is postsynaptic in nature^{83,85}. Future studies could additionally examine the PPR longer than presented here, to determine whether or not a change in PPR occurs long term.

In conclusion, we have displayed compelling evidence that *L*-Phe is a promiscuous molecule. *L*-Phe *dose* dependently activates galanin receptor type 1, resulting in an EC₅₀ of 754.4 μ M and is therefore a *bone fide* *L*-Phe receptor. Additionally, *L*-Phe decreases neuronal activity in the dorsomedial hypothalamus, specifically, neuronal excitability, glutamate transmission, and causes a long-term decrease in synaptic strength. This study has expanded our understanding of the effect of *L*-Phe signalling with G protein-coupled receptors, as well as its effects within the dorsomedial hypothalamus.

References

1. Zhao, J., Deng, Y., Jiang, Z., and Qing, H. (2016). G Protein-Coupled Receptors (GPCRs) in Alzheimer's Disease: A Focus on BACE1 Related GPCRs. *Frontiers in Aging Neuroscience* 8.
2. Lundstrom, K. (2005). Structural genomics of GPCRs. *Trends Biotechnol* 23, 103–108. 10.1016/j.tibtech.2004.12.006.
3. Santos, R., Ursu, O., Gaulton, A., Bento, A.P., Donadi, R.S., Bologa, C.G., Karlsson, A., Al-lazikani, B., Hersey, A., Oprea, T.I., et al. (2017). A comprehensive map of molecular drug targets. *Nature Reviews. Drug Discovery* 16, 19–34. 10.1038/nrd.2016.230.
4. Wacker, D., Stevens, R.C., and Roth, B.L. (2017). How ligands illuminate GPCR molecular pharmacology. *Cell* 170, 414–427. 10.1016/j.cell.2017.07.009.
5. Lu, S., Jang, W., Inoue, A., and Lambert, N.A. (2021). Constitutive G protein coupling profiles of understudied orphan GPCRs. *PLOS ONE* 16, e0247743. 10.1371/journal.pone.0247743.
6. Basith, S., Cui, M., Macalino, S.J.Y., Park, J., Clavio, N.A.B., Kang, S., and Choi, S. (2018). Exploring G Protein-Coupled Receptors (GPCRs) Ligand Space via Cheminformatics Approaches: Impact on Rational Drug Design. *Frontiers in Pharmacology* 9.
7. Harmor, A.J. (2001). Family-B G-protein-coupled receptors. *Genome Biol* 2, reviews3013.1-reviews3013.10.
8. Lee, Y., Basith, S., and Choi, S. (2018). Recent Advances in Structure-Based Drug Design Targeting Class A G Protein-Coupled Receptors Utilizing Crystal Structures and Computational Simulations. *J. Med. Chem.* 61, 1–46. 10.1021/acs.jmedchem.6b01453.
9. Zhou, Q., Yang, D., Wu, M., Guo, Y., Guo, W., Zhong, L., Cai, X., Dai, A., Jang, W., Shakhnovich, E.I., et al. (2019). Common activation mechanism of class A GPCRs. *eLife* 8, e50279. 10.7554/eLife.50279.
10. Rasmussen, S.G.F., DeVree, B.T., Zou, Y., Kruse, A.C., Chung, K.Y., Kobilka, T.S., Thian, F.S., Chae, P.S., Pardon, E., Calinski, D., et al. (2011). Crystal Structure of the β 2Adrenergic Receptor-Gs protein complex. *Nature* 477, 549–555. 10.1038/nature10361.
11. Dixon, R.A.F., Kobilka, B.K., Strader, D.J., Benovic, J.L., Dohlman, H.G., Frielle, T., Bolanowski, M.A., Bennett, C.D., Rands, E., Diehl, R.E., et al. (1986). Cloning of the gene and cDNA for mammalian β -adrenergic receptor and homology with rhodopsin. *Nature* 321, 75–79. 10.1038/321075a0.
12. De Lean, A., Stadel, J.M., and Lefkowitz, R.J. (1980). A ternary complex model explains the agonist-specific binding properties of the adenylate cyclase-coupled beta-

- adrenergic receptor. *Journal of Biological Chemistry* 255, 7108–7117. 10.1016/S0021-9258(20)79672-9.
13. Tuteja, N. (2009). Signaling through G protein coupled receptors. *Plant Signaling & Behavior* 4, 942–947. 10.4161/psb.4.10.9530.
 14. Nair, A., Chauhan, P., Saha, B., and Kubatzky, K.F. (2019). Conceptual Evolution of Cell Signaling. *Int J Mol Sci* 20, 3292. 10.3390/ijms20133292.
 15. Moepps, B., and Fagni, L. (2003). Mont Sainte-Odile: a sanctuary for GPCRs. *EMBO reports* 4, 237–243. 10.1038/sj.embor.embor777.
 16. Jean-Charles, P.-Y., Kaur, S., and Shenoy, S.K. (2017). GPCR signaling via β -arrestin-dependent mechanisms. *J Cardiovasc Pharmacol* 70, 142–158. 10.1097/FJC.0000000000000482.
 17. Luttrell, L.M., Ferguson, S.S.G., Daaka, Y., Miller, W.E., Maudsley, S., Della Rocca, G.J., Lin, F.-T., Kawakatsu, H., Owada, K., Luttrell, D.K., et al. (1999). β -Arrestin-Dependent Formation of β 2 Adrenergic Receptor-Src Protein Kinase Complexes. *Science* 283, 655–661. 10.1126/science.283.5402.655.
 18. van Gastel, J., Hendrickx, J.O., Leysen, H., Santos-Otte, P., Luttrell, L.M., Martin, B., and Maudsley, S. (2018). β -Arrestin Based Receptor Signaling Paradigms: Potential Therapeutic Targets for Complex Age-Related Disorders. *Frontiers in Pharmacology* 9.
 19. Lefkowitz, R.J., and Shenoy, S.K. (2005). Transduction of Receptor Signals by β -Arrestins. *Science* 308, 512–517. 10.1126/science.1109237.
 20. Zeghal, M., Laroche, G., and Giguère, P.M. (2020). Parallel Interrogation of β -Arrestin2 Recruitment for Ligand Screening on a GPCR-Wide Scale using PRESTO-Tango Assay. *J Vis Exp*. 10.3791/60823.
 21. Kroeze, W.K., Sassano, M.F., Huang, X.-P., Lansu, K., McCorvy, J.D., Giguere, P.M., Sciaky, N., and Roth, B.L. (2015). PRESTO-TANGO: an open-source resource for interrogation of the druggable human GPCR-ome. *Nat Struct Mol Biol* 22, 362–369. 10.1038/nsmb.3014.
 22. Barnea, G., Strapps, W., Herrada, G., Berman, Y., Ong, J., Kloss, B., Axel, R., and Lee, K.J. (2008). The genetic design of signaling cascades to record receptor activation. *Proc Natl Acad Sci U S A* 105, 64–69. 10.1073/pnas.0710487105.
 23. Thorne, N., Inglese, J., and Auld, D.S. (2010). Illuminating Insights into Firefly Luciferase and Other Bioluminescent Reporters Used in Chemical Biology. *Chemistry & Biology* 17, 646–657. 10.1016/j.chembiol.2010.05.012.
 24. Rudenko, O., Shang, J., Munk, A., Ekberg, J.P., Petersen, N., Engelstoft, M.S., Egerod, K.L., Hjorth, S.A., Wu, M., Feng, Y., et al. (2018). The aromatic amino acid sensor

- GPR142 controls metabolism through balanced regulation of pancreatic and gut hormones. *Mol Metab* *19*, 49–64. 10.1016/j.molmet.2018.10.012.
25. Strassheim, D., Sullivan, T., Irwin, D.C., Gerasimovskaya, E., Lahm, T., Klemm, D.J., Dempsey, E.C., Stenmark, K.R., and Karoor, V. (2021). Metabolite G-Protein Coupled Receptors in Cardio-Metabolic Diseases. *Cells* *10*, 3347. 10.3390/cells10123347.
 26. Parthasarathy, A., Cross, P.J., Dobson, R.C.J., Adams, L.E., Savka, M.A., and Hudson, A.O. (2018). A Three-Ring Circus: Metabolism of the Three Proteogenic Aromatic Amino Acids and Their Role in the Health of Plants and Animals. *Frontiers in Molecular Biosciences* *5*.
 27. Beckmann, H., Athen, D., Olteanu, M., and Zimmer, R. (1979). DL-phenylalanine versus imipramine: a double-blind controlled study. *Arch Psychiatr Nervenkr* (1970) *227*, 49–58. 10.1007/BF00585677.
 28. Bergwerff, C.E., Luman, M., Blom, H.J., and Oosterlaan, J. (2016). No Tryptophan, Tyrosine and Phenylalanine Abnormalities in Children with Attention-Deficit/Hyperactivity Disorder. *PLoS One* *11*, e0151100. 10.1371/journal.pone.0151100.
 29. Best, J.A., Nijhout, H.F., and Reed, M.C. (2009). Homeostatic mechanisms in dopamine synthesis and release: a mathematical model. *Theor Biol Med Model* *6*, 21. 10.1186/1742-4682-6-21.
 30. Flydal, M.I., and Martinez, A. (2013). Phenylalanine hydroxylase: Function, structure, and regulation. *IUBMB Life* *65*, 341–349. 10.1002/iub.1150.
 31. Blau, N., van Spronsen, F.J., and Levy, H.L. (2010). Phenylketonuria. *The Lancet* *376*, 1417–1427. 10.1016/S0140-6736(10)60961-0.
 32. Ballinger, A.B., and Clark, M.L. (1994). l-Phenylalanine releases cholecystokinin (CCK) and is associated with reduced food intake in humans: Evidence for a physiological role of CCK in control of eating. *Metabolism - Clinical and Experimental* *43*, 735–738. 10.1016/0026-0495(94)90123-6.
 33. Liou, A.P., Sei, Y., Zhao, X., Feng, J., Lu, X., Thomas, C., Pechhold, S., Raybould, H.E., and Wank, S.A. (2011). The extracellular calcium-sensing receptor is required for cholecystokinin secretion in response to l-phenylalanine in acutely isolated intestinal I cells. *American Journal of Physiology-Gastrointestinal and Liver Physiology* *300*, G538–G546. 10.1152/ajpgi.00342.2010.
 34. Prpic, V., Basavappa, S., Liddle, R.A., and Mangel, A.W. (1994). Regulation of Cholecystokinin Secretion by Calcium-Dependent Calmodulin Kinase II: Differential Effects of Phenylalanine and cAMP. *Biochemical and Biophysical Research Communications* *201*, 1483–1489. 10.1006/bbrc.1994.1871.

35. Crosby, K.M., Murphy-Royal, C., Wilson, S.A., Gordon, G.R., Bains, J.S., and Pittman, Q.J. (2018). Cholecystokinin Switches the Plasticity of GABA Synapses in the Dorsomedial Hypothalamus via Astrocytic ATP Release. *J. Neurosci.* 38, 8515–8525. 10.1523/JNEUROSCI.0569-18.2018.
36. Mastorakos, G., and Zapanti, E. (2004). The Hypothalamic-Pituitary-Adrenal Axis in the Neuroendocrine Regulation of Food Intake and Obesity: The Role of Corticotropin Releasing Hormone. *Nutritional Neuroscience* 7, 271–280. 10.1080/10284150400020516.
37. Ihnatko, R., and Theodorsson, E. (2017). Short N-terminal galanin fragments are occurring naturally in vivo. *Neuropeptides* 63, 1–13. 10.1016/j.npep.2017.03.005.
38. Kyrkouli, S.E., Glenn Stanley, B., and Leibowitz, S.F. (1986). Galanin: Stimulation of feeding induced by medial hypothalamic injection of this novel peptide. *European Journal of Pharmacology* 122, 159–160. 10.1016/0014-2999(86)90175-5.
39. Nagase, H., Nakajima, A., Sekihara, H., York, D.A., and Bray, G.A. (2002). Regulation of feeding behavior, gastric emptying, and sympathetic nerve activity to interscapular brown adipose tissue by galanin and enterostatin: the involvement of vagal-central nervous system interactions. *J Gastroenterol* 37, 118–127. 10.1007/BF03326430.
40. Mitchell, V., Bouret, S., Howard, A.D., and Beauvillain, J.-C. (1999). Expression of the galanin receptor subtype Gal-R2 mRNA in the rat hypothalamus. *Journal of Chemical Neuroanatomy* 16, 265–277. 10.1016/S0891-0618(99)00011-3.
41. Bellinger, L.L., and Bernardis, L.L. (2002). The dorsomedial hypothalamic nucleus and its role in ingestive behavior and body weight regulation: Lessons learned from lesioning studies. *Physiology & Behavior* 76, 431–442. 10.1016/S0031-9384(02)00756-4.
42. Chou, T.C., Scammell, T.E., Gooley, J.J., Gaus, S.E., Saper, C.B., and Lu, J. (2003). Critical Role of Dorsomedial Hypothalamic Nucleus in a Wide Range of Behavioral Circadian Rhythms. *J Neurosci* 23, 10691–10702. 10.1523/JNEUROSCI.23-33-10691.2003.
43. Jeong, J.H., Lee, D.K., and Jo, Y.-H. (2017). Cholinergic neurons in the dorsomedial hypothalamus regulate food intake. *Molecular Metabolism* 6, 306–312. 10.1016/j.molmet.2017.01.001.
44. Otgon-Uul, Z., Suyama, S., Onodera, H., and Yada, T. (2016). Optogenetic activation of leptin- and glucose-regulated GABAergic neurons in dorsomedial hypothalamus promotes food intake via inhibitory synaptic transmission to paraventricular nucleus of hypothalamus. *Mol Metab* 5, 709–715. 10.1016/j.molmet.2016.06.010.
45. Imoto, D., Yamamoto, I., Matsunaga, H., Yonekura, T., Lee, M.-L., Kato, K.X., Yamasaki, T., Xu, S., Ishimoto, T., Yamagata, S., et al. (2021). Refeeding activates

neurons in the dorsomedial hypothalamus to inhibit food intake and promote positive valence. *Mol Metab* 54, 101366. 10.1016/j.molmet.2021.101366.

46. Thompson, R. h., Canteras, N. s., and Swanson, L. w. (1996). Organization of projections from the dorsomedial nucleus of the hypothalamus: A PHA-L study in the rat. *Journal of Comparative Neurology* 376, 143–173. 10.1002/(SICI)1096-9861(19961202)376:1<143::AID-CNE9>3.0.CO;2-3.
47. Gooley, J.J., Schomer, A., and Saper, C.B. (2006). The dorsomedial hypothalamic nucleus is critical for the expression of food-entrainable circadian rhythms. *Nat Neurosci* 9, 398–407. 10.1038/nn1651.
48. Hetherington, A.W., and Ranson, S.W. (1940). Hypothalamic lesions and adiposity in the rat. *The Anatomical Record* 78, 149–172. 10.1002/ar.1090780203.
49. Rust, V.A., and Crosby, K.M. (2021). Cholecystokinin acts in the dorsomedial hypothalamus of young male rats to suppress appetite in a nitric oxide-dependent manner. *Neuroscience Letters* 764, 136295. 10.1016/j.neulet.2021.136295.
50. Mitchell, V., Habert-Ortoli, E., Epelbaum, J., Aubert, J.-P., and Beauvillain, J.-C. (1997). Semiquantitative Distribution of Galanin-Receptor (GAL-R1) mRNA-Containing Cells in the Male Rat Hypothalamus. *Neuroendocrinology* 66, 160–172. 10.1159/000127234.
51. Saar, I., Runesson, J., McNamara, I., Järv, J., Robinson, J.K., and Langel, Ü. (2011). Novel galanin receptor subtype specific ligands in feeding regulation. *Neurochemistry International* 58, 714–720. 10.1016/j.neuint.2011.02.012.
52. Pereda, A.E. (2014). Electrical synapses and their functional interactions with chemical synapses. *Nat Rev Neurosci* 15, 250–263. 10.1038/nrn3708.
53. Zhou, Y., and Danbolt, N. (2013). GABA and Glutamate Transporters in Brain. *Frontiers in Endocrinology* 4.
54. Dingledine, R., Borges, K., Bowie, D., and Traynelis, S.F. (1999). The Glutamate Receptor Ion Channels. *Pharmacol Rev* 51, 7–62.
55. Crupi, R., Impellizzeri, D., and Cuzzocrea, S. (2019). Role of Metabotropic Glutamate Receptors in Neurological Disorders. *Frontiers in Molecular Neuroscience* 12.
56. Crosby, K.M., Inoue, W., Pittman, Q.J., and Bains, J.S. (2011). Endocannabinoids gate state-dependent plasticity of synaptic inhibition in feeding circuits. *Neuron* 71, 529–541. 10.1016/j.neuron.2011.06.006.
57. Pastalkova, E., Serrano, P., Pinkhasova, D., Wallace, E., Fenton, A.A., and Sacktor, T.C. (2006). Storage of Spatial Information by the Maintenance Mechanism of LTP. *Science* 313, 1141–1144. 10.1126/science.1128657.

58. Yang, L., Scott, K.A., Hyun, J., Tamashiro, K.L., Tray, N., Moran, T.H., and Bi, S. (2009). Role of Dorsomedial Hypothalamic Neuropeptide Y in Modulating Food Intake and Energy Balance. *J. Neurosci.* 29, 179–190. 10.1523/JNEUROSCI.4379-08.2009.
59. Crosby, K.M., Baimoukhametova, D.V., Bains, J.S., and Pittman, Q.J. (2015). Postsynaptic Depolarization Enhances GABA Drive to Dorsomedial Hypothalamic Neurons through Somatodendritic Cholecystinin Release. *J Neurosci* 35, 13160–13170. 10.1523/JNEUROSCI.3123-14.2015.
60. Raybould, H.E. (2007). Mechanisms of CCK signaling from gut to brain. *Curr Opin Pharmacol* 7, 570–574. 10.1016/j.coph.2007.09.006.
61. Glushakov, A. v., Dennis, D. m., Sumners, C., Seubert, C. n., and Martynyuk, A. e. (2003). L-phenylalanine selectively depresses currents at glutamatergic excitatory synapses. *Journal of Neuroscience Research* 72, 116–124. 10.1002/jnr.10569.
62. Rourke, J.L., Muruganandan, S., Dranse, H.J., McMullen, N.M., and Sinal, C.J. (2014). Gpr1 is an active chemerin receptor influencing glucose homeostasis in obese mice. *J Endocrinol* 222, 201–215. 10.1530/JOE-14-0069.
63. Branchek, T., Smith, K.E., and Walker, M.W. (1998). Molecular Biology and Pharmacology of Galanin Receptors. *Annals of the New York Academy of Sciences* 863, 94–107. 10.1111/j.1749-6632.1998.tb10687.x.
64. Kask, K., Berthold, M., and Bartfai, T. (1997). Galanin receptors: Involvement in feeding, pain, depression and Alzheimer's disease. *Life Sciences* 60, 1523–1533. 10.1016/S0024-3205(96)00624-8.
65. Moreno, E., Vaz, S.H., Cai, N.-S., Ferrada, C., Quiroz, C., Barodia, S.K., Kabbani, N., Canela, E.I., McCormick, P.J., Lluís, C., et al. (2011). Dopamine–Galanin Receptor Heteromers Modulate Cholinergic Neurotransmission in the Rat Ventral Hippocampus. *J. Neurosci.* 31, 7412–7423. 10.1523/JNEUROSCI.0191-11.2011.
66. Reyes-Alcaraz, A., Lee, Y.-N., Son, G.H., Kim, N.H., Kim, D.-K., Yun, S., Kim, D.-H., Hwang, J.-I., and Seong, J.Y. (2016). Development of Spexin-based Human Galanin Receptor Type II-Specific Agonists with Increased Stability in Serum and Anxiolytic Effect in Mice. *Sci Rep* 6, 21453. 10.1038/srep21453.
67. Poole, E.I., Rust, V.A., and Crosby, K.M. (2020). Nitric Oxide Acts in the Rat Dorsomedial Hypothalamus to Increase High Fat Food Intake and Glutamate Transmission. *Neuroscience* 440, 277–289. 10.1016/j.neuroscience.2020.05.039.
68. Glushakov, A.V., Glushakova, O., Varshney, M., Bajpai, L.K., Sumners, C., Laipis, P.J., Embury, J.E., Baker, S.P., Otero, D.H., Dennis, D.M., et al. (2005). Long-term changes in glutamatergic synaptic transmission in phenylketonuria. *Brain* 128, 300–307. 10.1093/brain/awh354.

69. Hu, R., Cao, Q., Sun, Z., Chen, J., Zheng, Q., and Xiao, F. (2018). A novel method of neural differentiation of PC12 cells by using Opti-MEM as a basic induction medium. *Int J Mol Med* 41, 195–201. 10.3892/ijmm.2017.3195.
70. Chen, H., Nwe, P.-K., Yang, Y., Rosen, C.E., Bielecka, A.A., Kuchroo, M., Cline, G.W., Kruse, A.C., Ring, A.M., Crawford, J.M., et al. (2019). A forward chemical genetic screen reveals gut microbiota metabolites that modulate host physiology. *Cell* 177, 1217-1231.e18. 10.1016/j.cell.2019.03.036.
71. Hagrot, E., Oddsdóttir, H.Æ., Hosta, J.G., Jacobsen, E.W., and Chotteau, V. (2017). Poly-pathway model, a novel approach to simulate multiple metabolic states by reaction network-based model – Application to amino acid depletion in CHO cell culture. *Journal of Biotechnology* 259, 235–247. 10.1016/j.jbiotec.2017.05.026.
72. Wang, M., Yao, Y., Kuang, D., and Hampson, D.R. (2006). Activation of Family C G-protein-coupled Receptors by the Tripeptide Glutathione*. *Journal of Biological Chemistry* 281, 8864–8870. 10.1074/jbc.M512865200.
73. Webling, K., Runesson, J., Lang, A., Saar, I., Kofler, B., and Langel, Ü. (2016). Ala5-galanin (2–11) is a GAL2R specific galanin analogue. *Neuropeptides* 60, 75–82. 10.1016/j.npep.2016.08.008.
74. Schuck, P.F., Malgarin, F., Cararo, J.H., Cardoso, F., Streck, E.L., and Ferreira, G.C. (2015). Phenylketonuria Pathophysiology: on the Role of Metabolic Alterations. *Aging Dis* 6, 390–399. 10.14336/AD.2015.0827.
75. Pikal-Cleland, K.A., Rodríguez-Hornedo, N., Amidon, G.L., and Carpenter, J.F. (2000). Protein denaturation during freezing and thawing in phosphate buffer systems: monomeric and tetrameric beta-galactosidase. *Arch Biochem Biophys* 384, 398–406. 10.1006/abbi.2000.2088.
76. Tamura, K., Palmer, J.M., Winkelmann, C.K., and Wood, J.D. (1988). Mechanism of action of galanin on myenteric neurons. *Journal of Neurophysiology* 60, 966–979. 10.1152/jn.1988.60.3.966.
77. Herrling, P.L., Morris, R., and Salt, T.E. (1983). Effects of excitatory amino acids and their antagonists on membrane and action potentials of cat caudate neurones. *The Journal of Physiology* 339, 207–222. 10.1113/jphysiol.1983.sp014712.
78. Glushakov, A.V., Dennis, D.M., Morey, T.E., Sumners, C., Cucchiara, R.F., Seubert, C.N., and Martynyuk, A.E. (2002). Specific inhibition of N-methyl-D-aspartate receptor function in rat hippocampal neurons by L-phenylalanine at concentrations observed during phenylketonuria. *Mol Psychiatry* 7, 359–367. 10.1038/sj.mp.4000976.
79. Nance, D.M., Bromley, B., Barnard, R.J., and Gorski, R.A. (1977). Sexually dimorphic effects of forced exercise on food intake and body weight in the rat. *Physiol Behav* 19, 155–158. 10.1016/0031-9384(77)90173-1.

80. Sawin, E.A., Murali, S.G., and Ney, D.M. (2014). Differential Effects of Low-Phenylalanine Protein Sources on Brain Neurotransmitters and Behavior in C57Bl/6-Pahenu2 Mice. *Mol Genet Metab* *111*, 452–461. 10.1016/j.ymgme.2014.01.015.
81. Campbell, A.P., and Smrcka, A.V. (2018). Targeting G protein-coupled receptor signalling by blocking G proteins. *Nat Rev Drug Discov* *17*, 789–803. 10.1038/nrd.2018.135.
82. Huttenlocher, P.R. (2000). The neuropathology of phenylketonuria: human and animal studies. *Eur J Pediatr* *159 Suppl 2*, S102-106. 10.1007/pl00014371.
83. Melis, M., Pistis, M., Perra, S., Muntoni, A.L., Pillolla, G., and Gessa, G.L. (2004). Endocannabinoids Mediate Presynaptic Inhibition of Glutamatergic Transmission in Rat Ventral Tegmental Area Dopamine Neurons through Activation of CB1 Receptors. *J Neurosci* *24*, 53–62. 10.1523/JNEUROSCI.4503-03.2004.
84. Manita, S., Suzuki, T., Inoue, M., Kudo, Y., and Miyakawa, H. (2007). Paired-pulse ratio of synaptically induced transporter currents at hippocampal CA1 synapses is not related to release probability. *Brain Res* *1154*, 71–79. 10.1016/j.brainres.2007.03.089.
85. Fatt, P., and Katz, B. (1952). Spontaneous subthreshold activity at motor nerve endings. *J Physiol* *117*, 109–128.

Appendix

Table 1. Dilution of Galanin ligand in TBS at 3X concentration for PRESTO-Tango assay treatment. Galanin was diluted into serum free phenylalanine free DMEM, and 9mM phenylalanine DMEM (serum free).

Concentration Key	[Galanin] (μM)
A	3
B	1.5
C	0.75
D	0.38
E	0.18
F	$9.35 \cdot 10^{-2}$
G	$4.68 \cdot 10^{-2}$
H	$2.34 \cdot 10^{-2}$
I	$1.17 \cdot 10^{-2}$
J	$5.86 \cdot 10^{-2}$

Table 2. Dilution of phenylalanine into serum free phenylalanine free media at 3X concentration for PRESTO-Tango assay treatment.

Concentration Key	[L-Phenylalanine] (μM)
A	60,000
B	30,000
C	15,000
D	7,500
E	3,000
F	1,500
G	750
H	375
I	187.5
J	0

Table 3. Mean and significance values of galanin receptor 1 activation when treated with DMSO vs. TBS.

Galanin Treatment	Mean 1	Mean 2	Mean Difference	Standard error of the mean	p-value
0 μ M GAL in TBS vs. 1 μ M GAL in TBS	2.052	2.139	-0.08632	0.3084	>0.9999
0 μ M GAL in TBS vs. 10 μ M GAL in TBS	2.052	2.137	-0.08495	0.3084	>0.9999
0 μ M GAL in TBS vs. 0 μ M GAL in DMSO	2.052	2.074	-0.02167	0.3084	>0.9999
0 μ M GAL in TBS vs. 1 μ M GAL in DMSO	2.052	2.246	-0.1934	0.3084	0.9998
0 μ M GAL in TBS vs. 10 μ M GAL in DMSO	2.052	2.392	-0.3402	0.3084	0.9917
1 μ M GAL in TBS vs. 10 μ M GAL in TBS	2.139	2.137	0.001368	0.3084	>0.9999
1 μ M GAL in TBS vs. 0 μ M GAL in DMSO	2.139	2.074	0.06465	0.3084	>0.9999
1 μ M GAL in TBS vs. 1 μ M GAL in DMSO	2.139	2.246	-0.1071	0.3084	>0.9999
1 μ M GAL in TBS vs. 10 μ M GAL in DMSO	2.139	2.392	-0.2539	0.3084	0.9990
10 μ M GAL in TBS vs. 0 μ M GAL in DMSO	2.137	2.074	0.06329	0.3084	>0.9999
10 μ M GAL in TBS vs. 1 μ M GAL in DMSO	2.137	2.246	-0.1084	0.3084	>0.9999

10 μ M GAL in TBS vs. 10 μ M GAL in DMSO	2.137	2.392	-0.2552	0.3084	0.9990
0 μ M GAL in DMSO vs. 1 μ M GAL in DMSO	2.074	2.246	-0.1717	0.3084	0.9998
0 μ M GAL in DMSO vs. 10 μ M GAL in DMSO	2.074	2.392	-0.3185	0.3084	0.9939
1 μ M GAL in DMSO vs. 10 μ M GAL in DMSO	2.246	2.392	-0.1468	0.3084	0.9999

Table 4. Mean and significance values of galanin receptor 2 activation when treated with DMSO vs. TBS.

Galanin Treatment	Mean 1	Mean 2	Mean Difference	Standard error of the mean	p-value
0 μ M GAL in TBS vs. 1 μ M GAL in TBS	55.27	62.39	-7.121	35.40	>0.9999
0 μ M GAL in TBS vs. 10 μ M GAL in TBS	55.27	79.71	-24.44	35.40	>0.9999
0 μ M GAL in TBS vs. 0 μ M GAL in DMSO	55.27	75.30	-20.04	35.40	>0.9999
0 μ M GAL in TBS vs. 1 μ M GAL in DMSO	55.27	92.69	-37.43	35.40	0.9998
0 μ M GAL in TBS vs. 10 μ M GAL in DMSO	55.27	113.2	-57.89	35.40	0.9917
1 μ M GAL in TBS vs. 10 μ M GAL in TBS	62.39	79.71	-17.32	35.40	>0.9999
1 μ M GAL in TBS vs. 0 μ M GAL in DMSO	62.39	75.30	-12.91	35.40	>0.9999
1 μ M GAL in TBS vs. 1 μ M GAL in DMSO	62.39	92.69	-30.31	35.40	>0.9999
1 μ M GAL in TBS vs. 10 μ M GAL in DMSO	62.39	113.2	-50.77	35.40	0.9990
10 μ M GAL in TBS vs. 0 μ M GAL in DMSO	79.71	75.30	4.409	35.40	>0.9999
10 μ M GAL in TBS vs. 1 μ M GAL in DMSO	79.71	92.69	-12.98	35.40	>0.9999

10 μ M GAL in TBS vs. 10 μ M GAL in DMSO	79.71	113.2	-33.44	35.40	0.9990
0 μ M GAL in DMSO vs. 1 μ M GAL in DMSO	75.30	92.69	-17.39	35.40	0.9998
0 μ M GAL in DMSO vs. 10 μ M GAL in DMSO	75.30	113.2	-37.85	35.40	0.9939
1 μ M GAL in DMSO vs. 10 μ M GAL in DMSO	92.69	113.2	-20.46	35.40	0.9999